Pontificia Universidad Católica del Perú

Escuela de Posgrado

Optimal Control Algorithm Design for a Prototype of Active Noise Control System

Author:

Edgar André Manzano Ramos

Advisors:

Ph.D. Julio Cesar Tafur Sotelo
MSc. Jesus Alan Calderon Chavarri

Lima, Mar 2017

Abstract

High-level noise can represent a serious risk for the health, industrial operations often represent continuous exposure to noise, thus an important trouble to handle. An alternative of solution can be the use of passive mechanisms of noise reductions, nonetheless its application cannot diminish low-frequency noise.

Active Noise Control (ANC) is the solution used for low-frequency noise, ANC systems work according to the superposition principle generating a secondary anti-noise signal to reduce both.

Nevertheless, the generation of an anti-noise signal with same oppose characteristics of the original noise signal presupposes the utilization of special techniques such as adaptive algorithms. These algorithms involve computational costs.

The present research present the optimization of a specific ANC algorithm in the step-size criteria. Delayed Filtered-x LMS (FxLMS) algorithm using an optimal step-size is evaluated in a prototype of ANC system.

"To God, my parents, brother, sister and my grandmother Marta"

Acknowledgements

This little work was made with help of:
Mother, all of this is because of you.
My family in Puno, thanks for your love and support.
My family in Lima, especially Mrs. Dora and my Aunt Jacqui, thanks for all.
PUCP and Concytec, thanks for the opportunity.
Mr. Calderon, thank you for all your academic advise.

Acronyms

WHO World Health Organization
ANC Active Noise Control
SPL Sound Pressure Level
dB Decibels
dBA A-weighted Decibels
OSHA Occupational Safety and Health Administration
DRC Damage-Risk Criteria
NIOSH National Institute of Occupational Safety and Health
REL Recommended Exposure Limit
PEL Permissible Exposure Limit
NIHL Noise-Induced Hearing Loss
IIR Infinite Impulse Response
FIR Finite Impulse Response
A/D Analog to Digital
D/A Digital to Analog
FxLMS Filtered-x LMS
LMS Least Mean Square
FuLMS Filtered-U LMS
MVDR Minimum Variance Distortionless Response
MIR Magnetic Resonance Imaging
MR Magnetic Resonance
AWGN Additive White Gaussian Noise
SNR Signal to Noise Ratio
ADC Analog to Digital Converter

Contents

List of Figures

List of Tables

Introduction

Nowadays noise, which is regarded as an undesirable sound, that is generated by industrial processes has been recognized as a serious health hazard. According to the World Health Organization (WHO) guidelines, noise can cause adverse health effects such as hearing loss, sleep disturbances, and even cardiovascular problems.

Noise levels can be reduced by absorbing materials, which usually are used in passive strategies of noise control. These silencers are very effective in attenuating high frequencies noise; nevertheless, they are usually complex, expensive and ineffective at low frequencies. The reason is because at low frequencies the acoustic wavelengths become large compared to the thickness of a typical passive silences.

ANC proposes as a solution the use of an additional "anti-noise" signal that can attenuate noise level of the primary signal. Nonetheless, there are many targets to be achieved by ANC study. The key strategy is to identify the acoustic noise signal. Nowadays there are many algorithms which proposes the identification of it, unfortunately the majority requires a lot of computational burden.

The present research proposes the design of an Optimal Control Algorithm which minimizes the computational burden required in order to diminish effectively the noise in a prototype of ANC system.

In this thesis document, Chapter 1 presents important Theoretical Considerations of ANC. Consequently, State of the Art is developed in Chapter 2 to review the actual information of Single Frequency ANC systems.

Chapter 3 details the calculus of the optimal step-size in order to be evaluated in the Delayed FxLMS algorithm, for this purpose, previously it is analysed the stability

conditions of the algorithm in relationship with the step-size. Chapter 4 describes simulations and experimental tests developed in the prototype of ANC system built by Alan Calderon [CC15].

This thesis work lets has the future aim of optimize noise control by active mechanism through the successfully design, simulation, test and validation in real systems.

Chapter 1
Theoretical Considerations

1.1 Human Perception of Sound

Beranek and Mellow in [BM12] define sound as the following way: *"A sound is said to exist if a disturbance propagated through an elastic material causes an alteration in pressure or a displacement of the particles of the material which can be detected by a person or by an instrument"*

According to the concept above, Weber-Fechner affirm that perception of sound is proportional to the logarithmic value of sound pressure, is for that reason that it is generally represented as Sound Pressure Level (SPL) in the logarithmic way of Decibels (dB) [Mös09]. Table 1.1 shows this representation with some examples.

Table 1.1: Relation between the Sound pressures and the Sound pressure levels.

Sound pressure $p(N/m^2, rms)$	SPL $L(dB)$	Situation / Description
2×10^{-5}	0	hearing threshold
2×10^{-4}	20	forests, light winds
2×10^{-3}	40	library
2×10^{-2}	60	office
2×10^{-1}	80	traffic
2×10^{0}	100	hooter
2×10^{1}	120	jet takeoff
2×10^{2}	140	pain threshold

Source: [Mös09]

Nevertheless, human perception of sound presents different responses to sound pressures at different frequencies [Mös09]. Therefore, the A-weighting is used to adequately represent the sound perception that our hearing system recognizes [Mös09]. This response in A-weighted Decibels (dBA) has been represented in Fig. 1.1 for a spectrum of human audible frequencies.

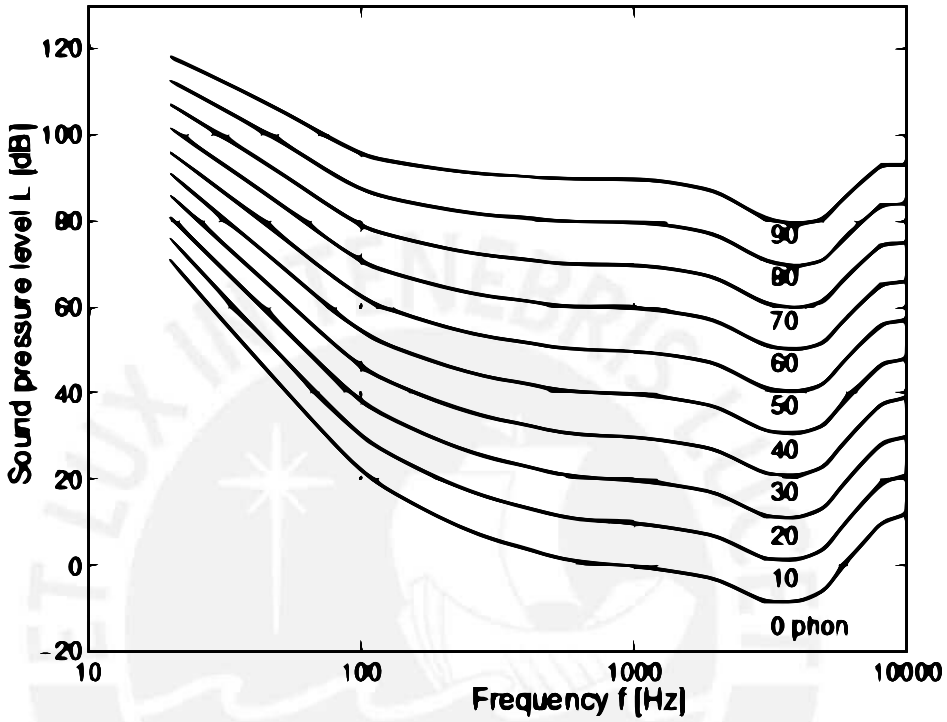

Figure 1.1: Hearing levels.
Source: [Mös09]

In this part is important to deliminated that human hearing range is located approximately between 20 Hz to 20 kHz. Nonetheless, sensibility to high frequencies decreases with the age and another factors, a lot of adult people cannot hear sounds above of 8 kHz [Sny12].

1.2 Noise effects

Acoustic noise is considered as an undesired and even offensive sound [BH09] [Pir15]. Nowadays, transport systems, electronic devices, medical equipment and other human activities are important noise sources. Nonetheless, the main problem is presented in industrial activities where devices such as fans, engines, blowers, transformers and others have converted the noise in a seriously risk to the health [BH09] [Sny12] [KGK12]. According to the guidelines of the WHO, noise can cause health

effects such as hearing loss, sleep disturbances and even cardiovascular problems [Egg13].

National Institute of Occupational Safety and Health (NIOSH) recommends a maximum exposure level of 85 dBA for a period of 8 hours. According to the Damage-Risk Criteria (DRC) by Occupational Safety and Health Administration (OSHA) (1981) the exposure level during 8 hours should be 90 dBA, and an increase of 5 dBA would imply a reduction of exposure time to 4 hours [Egg13].

OSHA Permissible Exposure Limit (PEL) allows 95 dBA during 4 hours and 100 dBA in 2 hours. In contrast, NIOSH Recommended Exposure Limit (REL) allows only 15 minutes for 100 dBA. DRC of OSHA affirms that 25% of exposed people to noise, according to PEL, are going to suffer Noise-Induced Hearing Loss (NIHL) with some years of regular exposure [Egg13].

1.3 Passive Techniques of Noise Reduction

Strategies considered as passive techniques of noise control or reduction are those that are based in the utilization of materials that absorb or reflect acoustic noise and cannot generate energy themselves [Pir15].

These techniques include equipment enclosure, use of barriers, silencers, further are considered the utilization of personal protection equipment such as ear-mufflers and ear-pluggers by the workers and other exposed people [BH09] [KGK12].

Passive techniques can reduce the noise in a wide range of frequencies. Nonetheless, have an important disadvantage in low-frequencies due their implementations are normally complex, expensive, bulky and in some cases ineffective [Sia12] [Fuc13].

1.4 ANC principle

In 1936, Lueg realized the first patent of ANC; it consisted in a system formed by a microphone and an electronically controlled loudspeaker that generate an anti-noise signal to diminish the acoustic noise. Nowadays, ANC systems involve a variety of algorithms, designs and applications, thus, publication of hundreds of articles per year, dozens of specialized companies, hundreds of patents and a wide study by universities and laboratories in the world [Pir15] [KGK12] [HSQ+12].

ANC systems are based in the superposition principle to sum a primary noise signal

and a secondary anti-noise signal, which is the most possible similar to the inverse of the primary signal, obtaining as a result the suppression of both signals due to the destructive interference principle [Mös09] [Pir15] [KKG10].

1.5 ANC Advantages and Disadvantages

1.5.1 Advantages

- ANC systems are effective with low-frequencies signals (approximately < 600 Hz), the passive techniques of reduction are ineffective with those frequencies.
- In addition, they can work with high-frequencies noise signals.
- Compact, modular and flexible systems.
- Potential benefits respect to volume, weight and cost.
- ANC systems do not imply physical modifications in the noise sources.
- ANC systems can attenuate 30 dB or more in narrowband noise signals and 15 to 20 dB in broadband noise signals.

1.5.2 Disadvantages

- ANC systems are least efficient in complex environments.
- ANC focus specific regions, it can produce unwanted effects of noise amplification in another regions.
- Frequency response of sensors and actuator can reduce the performance of the ANC systems.

1.6 Adaptive Filters

Adaptive filters are important elements in ANC systems; they are linear dynamic systems that present adaptive or variable structure and parameters.

Adaptive filtering have as fundamental process digital filtering and adaptation, which consists in the estimation of parameters or filter coefficients. General characteristics of filter will depend specially of filter structure and cost function used in the adaptation process [KBM13].

1.6.1 IIR Filters

Fig. 1.2 schemes the structure of an IIR recursive filter, $\widehat{y}(k)$ represents the output signal.

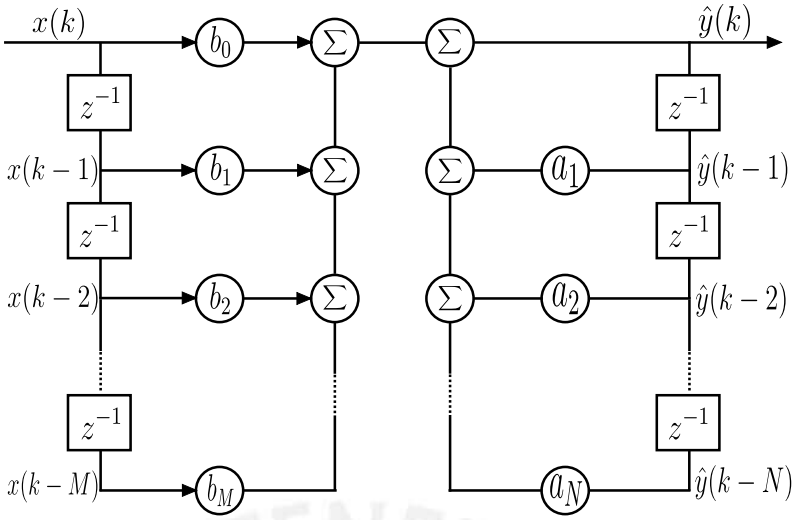

Figure 1.2: Structure of an IIR recursive filter.
Source: [KBM13]

In addition, equation (1.1) shows how calculate $\widehat{y}(k)$, the adaptive filter should update M parameters a_j and N parameters b_i. Is important to mention that parameters update represents a more complex operation in IIR filters than in FIR filters due to the instability trend [KBM13].

$$\widehat{y}(k) = \sum_{i=0}^{M} b_i(k)x(k-i) + \sum_{j=1}^{N} a_j(k)\widehat{y}(k-j) \tag{1.1}$$

Equation (1.1) can be represented as (1.2).

$$\widehat{y}(k) = \mathbf{B}_k(z^{-1})x(k) + (1 - \mathbf{A}_k(z^{-1}))\widehat{y}(k) \tag{1.2}$$

Where $\mathbf{B}_k(z^{-1})$ and $\mathbf{A}_k(z^{-1})$ are determined by equation (1.3).

$$\mathbf{B}_k(z^{-1}) = \sum_{i=0}^{M} b_i(k)z^{-i}; \mathbf{A}_k(z^{-1}) = 1 - \sum_{j=1}^{N} a_j(k)z^{-j} \tag{1.3}$$

From equation (1.2) is obtained relationship (1.4).

$$\mathbf{A}_k(z^{-1})\widehat{y}(k) = \mathbf{B}_k(z^{-1})x(k) \tag{1.4}$$

If it is assumed that filter parameters are time invariant, it is obtained filter transference function (1.5).

$$G(z) = \frac{Z[\widehat{y}(k)]}{Z[x(k)]} = \frac{\widehat{Y}(z)}{X(z)} = \frac{\mathbf{B}(z^{-1})}{\mathbf{A}(z^{-1})} \tag{1.5}$$

1.6.2 FIR Filters

A proposed solution to overcome potential instability of IIR filters is design a filter that present only zeros in order to achieve stability, recursive structure of the IIR filters should change to one that only has one direct tie or a non-recursive structure. Memory of these filters is limited, is for that reason denomination of FIR [KBM13], Fig. 1.3 represents mentioned structure.

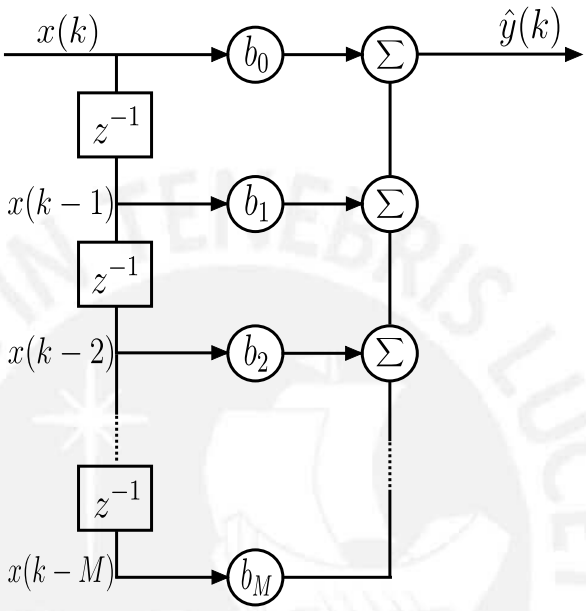

Figure 1.3: FIR filter structure

Source: [KBM13]

Output signal of the filter is defined by the linear equation of differences (1.6).

$$\widehat{y}(k) = \sum_{i=0}^{M} b_i(k)x(k-i) \tag{1.6}$$

It can be represented as simplified equation (1.7).

$$\widehat{y}(k) = \mathbf{B}_k(z^{-1})x(k) \tag{1.7}$$

Where M represents the filter order in equation (1.8).

$$\mathbf{B}_k(z^{-1}) = \sum_{i=0}^{M} b_i(k)z^{-i} \tag{1.8}$$

If the system is stationary or time invariant, transfer function will be defined as equation (1.9).

$$G(z) = \frac{Z[\widehat{y}(k)]}{Z[x(k)]} = \frac{\widehat{Y}(z)}{X(z)} = \frac{z^M \mathbf{B}(z^{-1})}{z^M} \tag{1.9}$$

1.7 ANC systems

An ANC system is based in the generation of an identical inverse signal to the noise signal, to get this it generally works with FIR adaptive filters to generate the mentioned "anti-noise" signal from the information of the noise and error signal. ANC systems are detailed in the present section.

1.7.1 Feedforward ANC systems

Feedforward ANC systems can be divided in two semi-groups: Broadband and Narrowband systems, where the most important difference is the Bandwidth of operation, for this reason Broadband systems work with more stochastic noise and use acoustic sensors, as long as Narrowband systems work with periodic noise and employ non-acoustic sensors.

Generally Feedforward ANC systems use one reference sensor (commonly a microphone for Broadband systems) to obtain the noise primary signal, one loudspeaker to generate the anti-noise secondary signal and one error sensor to get the residual noise that will be used for the updating of the adaptive filter [KGK12]. Fig. 1.4 shows this concept in a Broadband Feedforward ANC system diagram.

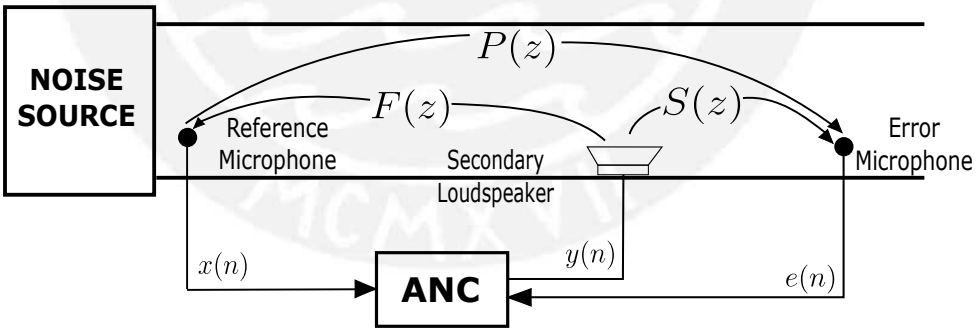

Figure 1.4: Feedforward ANC System Diagram.

Source: [AAK07]

In order to Broadband ANC systems work properly, signals from microphones should pass through pre-amplification, anti-aliasing filtering and Analog to Digital (A/D) conversion for their processing. As the same way, control signal to loudspeaker should pass through Digital to Analog (D/A) conversion, reconstruction filtering and amplification.

Fig. 1.5 detail the block diagram for an Broadband Feedforward ANC system where the reference signal $x(n)$ is detected by the reference microphone and the residual noise $e(n)$ is detected by the error microphone, consequently they pass to be processed by the adaptive filter $W(z)$, generating an anti-noise signal $y(n)$.

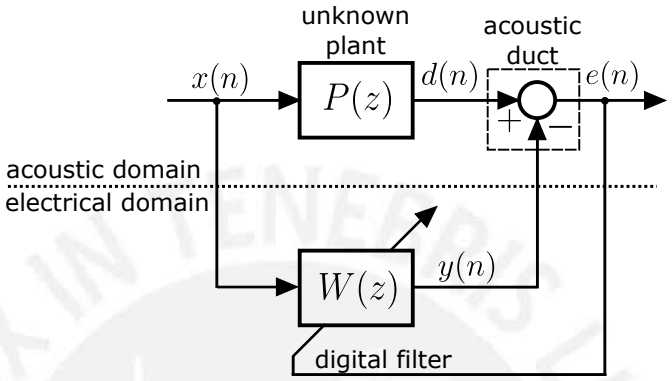

Figure 1.5: Feedforward ANC System Block Diagram
Source: [Pir15]

FxLMS algorithm

An important detail of Broadband Feedforward ANC system is that the effect of the circuits where are performed all the processing functions is represented by one transfer function denominated "secondary path". Therefore, selection of adaptive algorithm should consider this effect. In order to get a solution for the mentioned drawback, FxLMS algorithm was developed [GRMP13].

Nevertheless, Fig. 1.5 does not consider secondary path $S(z)$ that resume all the stages where the signal $y(n)$ pass until be emitted by the loudspeaker, loudspeaker response, loudspeaker to error microphone path, microphone error response and stages through which it passes this error signal $e(n)$ till enter to the adaptive filter.

In contrast, Fig. 1.6 considers secondary path $S(z)$ and the algorithm Least Mean Square (LMS) connected with the adaptive filter $W(z)$. Scheme is represented by equation (1.10).

$$E(z) = [P(z)X(z) - S(z)Y(z)]E(z) = [P(z) - S(z)W(z)]X(z) \tag{1.10}$$

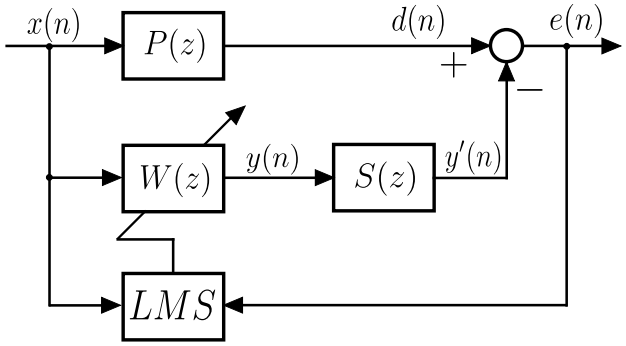

Figure 1.6: Feedforwad ANC System Block Diagram considering secondary path $S(z)$.
Source: [Pir15]

For an ideal case error will be null ($E(z) = 0$), obtaining (1.11) as solution (Optimal Transfer Function), dependence of the secondary path is evident.

$$W^{\circ}(z) = \frac{P(z)}{S(z)} \tag{1.11}$$

Effect produced by the response of the secondary path $S(z)$ tends to generate instability in the LMS algorithm, that can be deduced from the transfer function obtained in the equation (1.11). The proposed solution implies the utilization of an filter $\widehat{S}(z)$, identical to $S(z)$ in reference signal path in order to update filter coefficients considering the secondary path effect, this method of solution is denominated as FxLMS algorithm and Fig. 1.7 shows a block diagram that resumes it [Pir15] [KGK12].

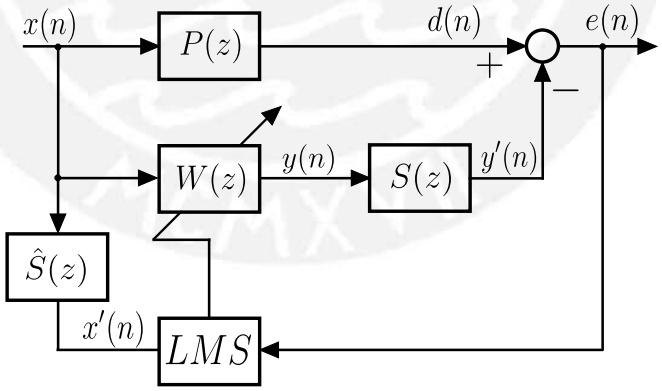

Figure 1.7: FxLMS Broadband Feedforward ANC Block Diagram
Source: [Pir15]

Equation (1.12) can be deduced from Fig. 1.7.

$$e(n) = d(n) - y'(n) = d(n) - s(n) * y(n) = d(n) - s(n) * [w(n)^T x(n)] \tag{1.12}$$

Where $s(n)$ represents impulse response of $S(z)$, $w(n) = [w_0(n)w_1(n)...w_{L-1}(n)]^T$ impulse response of $W(z)$ and $x(n) = [x(n)x(n-1)...x(n-L+1)]^T$ represents the reference signals vector for a L order filter.

LMS algorithm uses equation (1.13) to minimize the stochastic gradient.

$$w(n+1) = w(n) - \frac{\mu}{2}\nabla\widehat{J}(n) = w(n) - \frac{\mu}{2}\nabla(e^2(n)) = w(n) - \mu[\nabla e(n)]e(n) \quad (1.13)$$

Approximation of the gradient is referred by equation (1.14).

$$\nabla e(n) = -s(n) * x(n) = -x'(n) \quad (1.14)$$

Coefficients updating of the filter $W(z)$ is similar to LMS, with the difference that in this part is considering the transfer function $S(z)$ for weighting (1.15).

$$w(n+1) = w(n) + \mu x'(n)e(n) \quad (1.15)$$

One important observation is that this algorithm will can compensate the estimation errors of $S(z)$ with the condition that μ is enough small and the phase error between $S(z)$ and $\widehat{S}(z)$ does not exceed the 90° [Pir15] [KGK12].

1.7.2 Feedback ANC systems

On the other hand, Feedback ANC systems require only one sensor of the error signal (microphone) compared to Feedforward ANC systems and one secondary source of anti-noise (loudspeaker), it is not necessary a sensor for the primary noise signal because the algorithm focuses the error [KGK12]. Fig. 1.8 presents this idea.

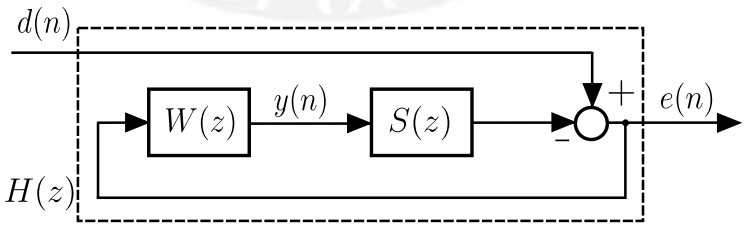

Figure 1.8: Feedback ANC System Block Diagram

Source: [Pir15]

Feedback ANC systems are generally applied where is not possible or is really hard to sense and obtain the noise signal with an acoustic or non-acoustic sensor, the key

element of Feedforward ANC systems [KGK12].

Furthermore, Feedback ANC systems are normally considered as non-adaptive due these only works with the error negative feedback. Table 1.2 makes a comparison between general adaptive Feedforward ANC and non-adaptive Feedback ANC systems.

Table 1.2: Comparative Table: Adaptive Feedforward and Non-adaptive Feedback ANC systems.

System	Advantages	Disadvantages
Adaptive Feedforward ANC	· Error signal controlled · Wide margins of stability · Accurate modeling is not required	· Difficult transient suppression · Coherent reference signal required
Non-adaptive Feedback ANC	· No reference microphone · No acoustic feedback · Transient suppression · Relatively simple control	· Not guaranteed stability · non-selective attenuation · Limitations Control Set · It requires accurate modeling

Source: [Pir15]

Hence, ANC Feedback adaptive systems are proposed through the estimation of the primary signal, thus these techniques are similar to Feedforward ANC systems, as is showed in Fig. 1.9 [Pir15].

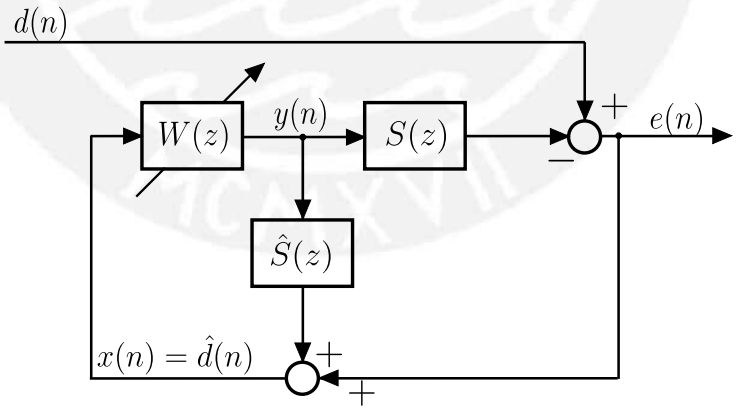

Figure 1.9: Adaptive Feedback ANC System Block Diagram.
Source: [Pir15]

For this reason, Feedback and Feedforwad ANC adaptive systems usually use FxLMS algorithm to reduce the effect of the secondary path. Fig. 1.10 shows a Feedback ANC system using FxLMS algorithm [Pir15].

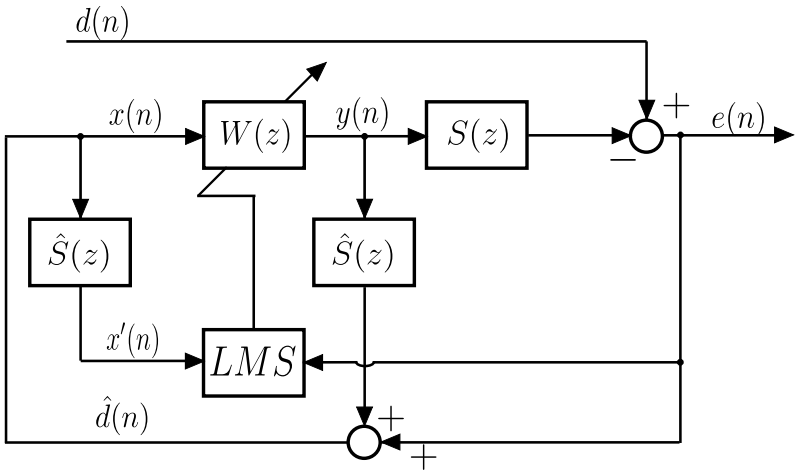

Figure 1.10: FxLMS Feedback ANC System Block Diagram.

Fuente: [Pir15]

1.7.3 Hybrid ANC systems

Hybrid ANC system is the combination of Feedforward and Feddback ANC systems, Fig. 1.11 shows the main idea of this structure.

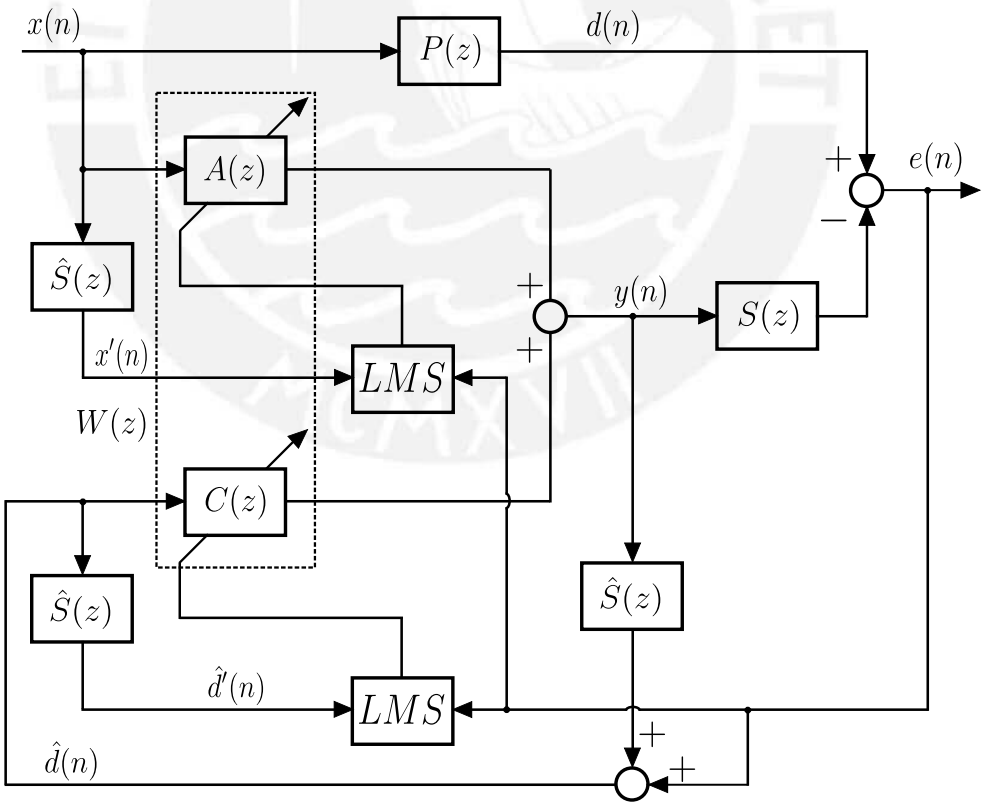

Figure 1.11: Hybrid ANC System Block Diagram using a FIR filters

Source: [KGK12]

Hybrid ANC systems perform a double cancellation based in the processing of the Feedforward and Feedback ANC subsystems. Hence, Hybrid ANC systems have more balanced performance that these, this idea can be resumed in the Table 1.3. Despite the fact, that the hybrid algorithm had long settling time, the settling time of the feedback algorithm is longer and the hybrid ANC systems were more stable to disturbances [CC15].

Table 1.3: Algorithm Comparison.

Algorithm	Settling time	Disturbance reject
Feedforward	short	bad
Hybrid	average	average
Feedback	long	good

Source: [CC15]

Chapter 2

State of the Art

The present research focuses the optimization of a Single Frequency ANC system, which is categorized as a Narrowband Feedforward ANC system.

2.1 Narrowband Feedforward ANC systems

Narrowband ANC systems are generally used by applications where noise is limited to a small group of frequencies. The main applications are focussed in motors, compressors, fans and rotational machines [Pir15]. Fig. 2.1 shows the structure of the system.

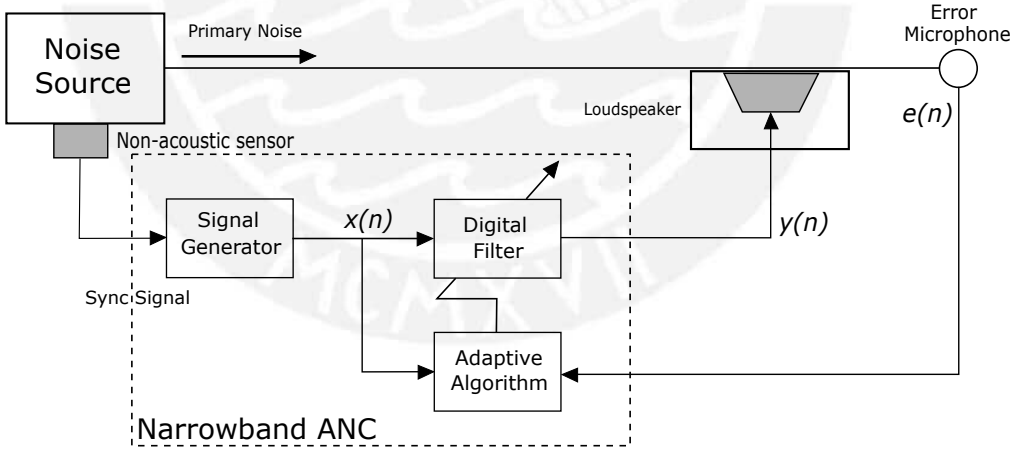

Figure 2.1: Narrowband ANC System Diagram.

Source: [Pir15]

The principle of operation of this structure is similar to Broadband Feedforward ANC system. It uses one loudspeaker to cancel the noise and one microphone to obtain the acoustic residual error, the main difference is that in order to get the reference signal (primary signal) it uses a non-acoustic sensor such as accelerometers

or tachometers. Consequently, it requires a signal generator to convert the lecture of the sensor for its processing in the controller [Pir15].

The main advantages of use Narrowband ANC systems are [Pir15]:

- There is not acoustic feedback of the reference microphone.
- Narrowband ANC systems avoid non-linear response of the microphones.
- It can control independently individual harmonics.

Unfortunately, non-acoustic sensors can present errors due fatigue, error that can generate misadjusts in the signal generator decreasing the system performance [KGK12].

2.2 Multi-frequency Feedforward ANC systems

In practice applications, periodic noise always present multiple harmonics and operation of multiple notches to reduce this drawback require high-order filters. Multi-frequency ANC systems diminish these signals by the use of multiple notches that can be implemented at the Direct, Parallel, Direct/Parallel and Cascade forms [CC15]. These notches operate single frequency signals (sinusoidal), generally are known as Adaptive Notch Filters or Cancellers.

2.3 Adaptive Notch Filters

When an ANC system is used in order to diminish a sinusoidal reference signal (Single Frequecy ANC), this is called as Adaptive Notch Filter. *"The advantages of the Adaptive Notch filter are that it offers easy control of Bandwith, an infinity null, and the capability to adaptively track the exact frequency of the interference in order to get a good performance for ANC"* [KM99]. Fig. 2.2 shows a single frequency adaptive Notch filter proposed by Kuo and Morgan in [KM99].

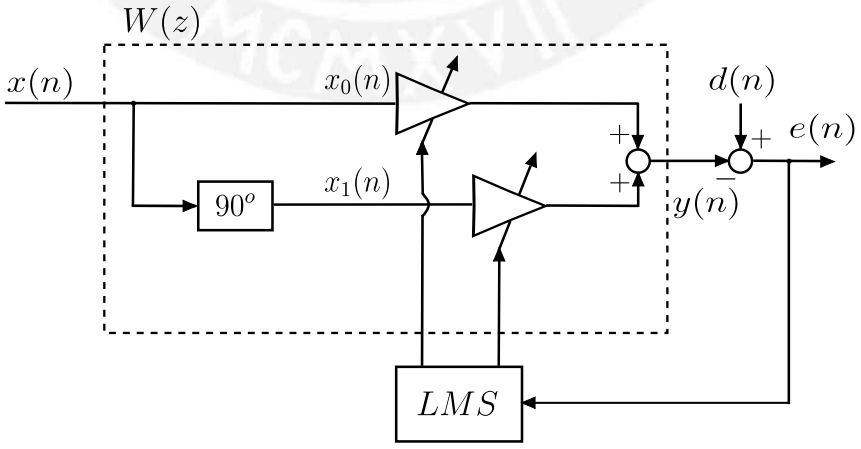

Figure 2.2: Single-frequency Adaptive Notch Filter.
Source: [KM99]

2.3.1 Analysis of Adaptive Notch Filters

The present analysis was developed by Widrow *et al* in [WGM+75]. For this purpose, $x(n)$ is considered the reference sinusoidal signal and is represented by the expression (2.1) where $t = nt_s$.

$$x(n) = A\cos(\omega_0 t) \tag{2.1}$$

Therefore, n-th references are represented by expressions (2.2) and (2.3).

$$x_0(n) = A\cos(\omega_0 n t_s + \phi) \tag{2.2}$$

$$x_1(n) = A\sin(\omega_0 n t_s + \phi) \tag{2.3}$$

And the n-th filter weightings are expressed by (2.4) and (2.5). Where μ is the step-size of the adaptive algorithm.

$$w_0(n+1) = w_0(n) + \mu e(n) x_0(n) \tag{2.4}$$

$$w_1(n+1) = w_1(n) + \mu e(n) x_1(n) \tag{2.5}$$

In order to obtain the transfer function of the Adaptive Notch Canceller, impulse response is analyzed for the system schemed by the flow diagram in Fig. 2.3.

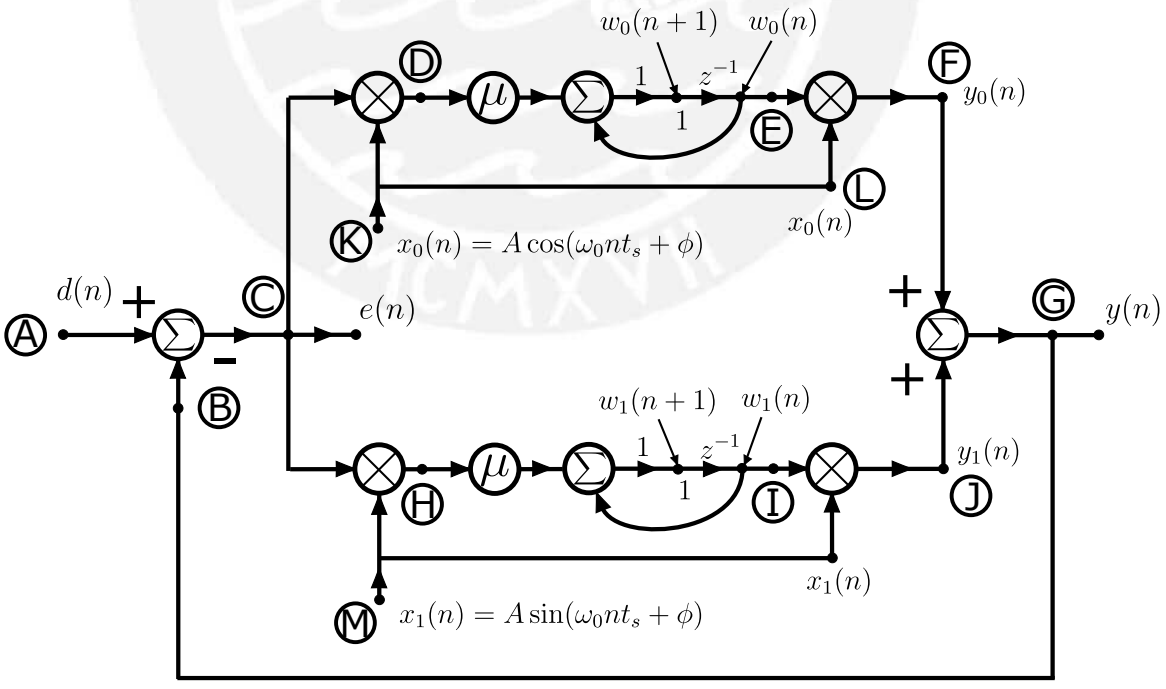

Figure 2.3: Flow diagram showing signal propagation in single-frequency adaptive notch canceler [WGM+75]

It is considered an impulse function described by equations (2.6) and (2.7) in point C, where α represents the amplitude of the impulse function.

$$e(n) = \alpha\delta(n-k) \tag{2.6}$$

$$\delta(n-k) = \begin{cases} 1 & for \quad n = k \\ 0 & for \quad n \neq k \end{cases} \tag{2.7}$$

Equation (2.8) details the expression achieved in point D. Is similar for point H with the difference of sin instead of cos .

$$e(n)x_0(n) = \begin{cases} \alpha A\cos(\omega_0 k t_s) & for \quad n = k \\ 0 & for \quad n \neq k \end{cases} \tag{2.8}$$

Analysis of the branch between points D and F, it is found the expression (2.9) for the filter weighting $w_0(n)$ in point E.

$$w_0(n) = \mu\alpha A\cos(\omega_0 k t_s + \phi) \tag{2.9}$$

Where $n \geqslant k+1$, due convolution operated in the branch between μ and $x_0(n)$ and the step function $u(n-1)$ corresponding to the delay z^{-1}. Therefore, expression (2.10) is obtained in point F.

$$y_0(n) = \mu\alpha A^2\cos(\omega_0 n t_s + \phi)\cos(\omega_0 k t_s + \phi) \tag{2.10}$$

At the same way, $y_1(n)$ is expressed in the point J by (2.11).

$$y_1(n) = \mu\alpha A^2\sin(\omega_0 j t_s + \phi)\sin(\omega_0 k t_s + \phi) \tag{2.11}$$

Hence, $y(n)$ is expressed by equation (2.12).

$$y(n) = y_0(n) + y_1(n) = \mu\alpha A^2 cos(\omega_0 t_s(n-k)) \tag{2.12}$$

Considering the step function, we obtain expression (2.13).

$$y(n) = \mu\alpha A^2 u((n-k)-1)\cos(\omega_0 t_s(n-k)) \tag{2.13}$$

Considering an impulse unitary function ($\alpha = 1$) in $k = 0$, it is obtained the expression (2.14).

$$y(n) = \mu A^2 u(n-1)\cos(\omega_0 n t_s) \tag{2.14}$$

Therefore, transfer function for this path is expressed by (2.15).

$$G(z) = \mu A^2 \left[\frac{z(z-\cos(\omega_0 t_s))}{z^2 - 2z\cos(\omega_0 t_s) + 1} - 1\right] \tag{2.15}$$

Considering the angular sampling frequency $\Omega = 2\pi/t_s$, (2.16) is obtained.

$$G(z) = \frac{\mu A^2[z\cos(2\pi\omega_0\Omega^{-1}) - 1]}{z^2 - 2z\cos(2\pi\omega_0\Omega^{-1}) + 1} \tag{2.16}$$

When feedback loop is closed from point G to point B, it is obtained transfer function $H(z)$ from the point A to point C in expression (2.17).

$$H(z) = \frac{E(z)}{D(z)} = \frac{z^2 - 2z\cos(2\pi\omega_0\Omega^{-1}) + 1}{z^2 - (2-\mu A^2)z\cos(2\pi\omega_0\Omega^{-1}) + 1 - \mu A^2} \tag{2.17}$$

Widrow *et al* in [WGM+75], analyses the properties of the notch canceler at the reference frequency w_0. The *zeros* are located at the Z plane in (2.18), and the poles in (2.19). And both are into the unit circle that mark the stability of our system, showed in Fig. 2.4.

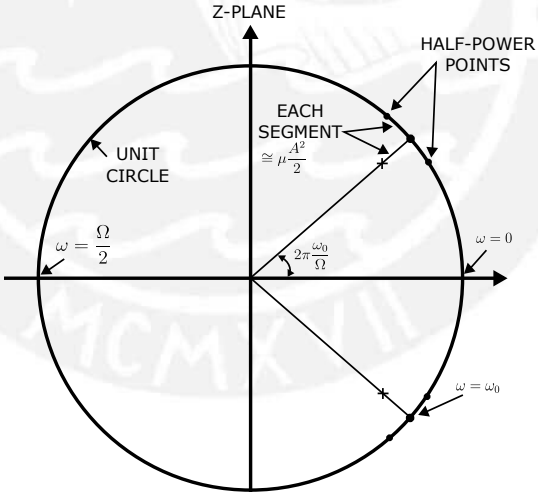

Figure 2.4: Location of poles and zeros [WGM+75]

$$z = e^{\pm i 2\pi\omega_0\Omega^{-1}} \tag{2.18}$$

$$p = (1 - \frac{\mu A^2}{2})\cos(2\pi\omega_0\Omega^{-1}) \pm i[(1-\mu A^2) - (1-\frac{\mu A^2}{2})\cos^2(2\pi\omega_0)\Omega^{-1}]^{1/2} \tag{2.19}$$

Poles are inside of the circle with a radial distance of approximately $1 - \frac{\mu A^2}{2}$.
In a frequency response analysis, it is obtained the expression (2.20) and Fig. 2.5 for the Bandwidth formula and frequency response image.

$$B \approx \frac{\mu A^2 \Omega}{2\pi} \tag{2.20}$$

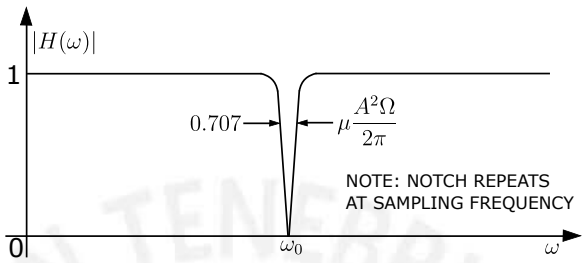

Figure 2.5: Magnitude of Transfer Function [WGM+75]

Kuo and Morgan in [KM99], shows a little different expression for (2.17) in (3.1), where is not considered the sampling variables.

$$H(z) = \frac{E(z)}{D(z)} = \frac{z^2 - 2z\cos(\omega_0) + 1}{z^2 - (2 - \mu A^2)z\cos(\omega_0) + 1 - \mu A^2} \tag{2.21}$$

2.4 Delayed FxLMS ANC

Adaptive Notch Filters represent a special case of Narrowband ANC systems, and how any ANC secondary path effect is an important drawback. Ziegler in [ZJ89] develops a simplified version of FxLMS algorithm in this specific case denominated Delayed FxLMS algorithm.

Equation (2.22) presents Delayed FxLMS algorithm, the purpose of the delay (Δ) is to align the reference signal to the error signal in order to update the filter weights to minimize the residual error [Han02], additionally Kuo and Morgan in [KM99] consider it as a compensation to the secondary path effect.

$$w_l(n+1) = w_l(n) + \mu e(n) x_l(n - \Delta) \tag{2.22}$$

Where $l = 0$ or $l = 1$.

According to [KM99], the delay unit can be replaced by the a secondary path estimate of $S(z)$ as is shown in the Fig. 3.6.

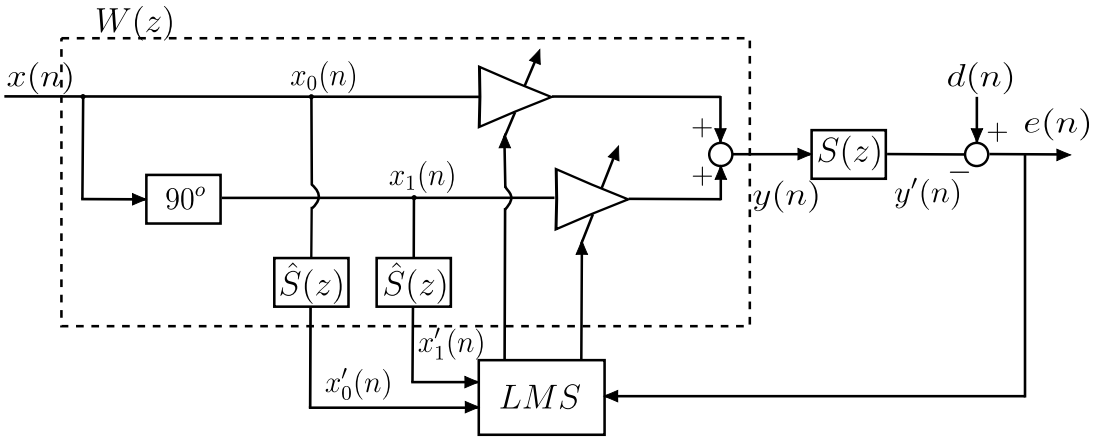

Figure 2.6: Delayed FxLMS ANC.

Source: [KM99]

Now, the adaptive weights are update by equation (2.23).

$$w_l(n+1) = w_l(n) + \mu e(n) x'_l(n) \tag{2.23}$$

where $l = 0$ or $l = 1$.

Considering $x'_l(n)$ as a modified version of $x_l(n - \Delta)$ from equation (2.22). Their relationship is showed by equation (2.24).

$$x'_l(n) = A_s x_l(n - \Delta) \tag{2.24}$$

where A_s is the amplitude of $S(z)$ (estimate)

The transfer function proposed by [KM99] of the Narrowband ANC system is given by expression (2.25), it considers the secondary path $S(z)$ and its identification $\hat{S}(z)$ effects.

$$H(z) = \frac{z^2 - 2z\cos(\omega_0) + 1}{z^2 - [2\cos(\omega_0) - \beta\cos(\omega_0 - \phi_\Delta)]z + 1 - \beta\cos(\phi_\Delta)} \tag{2.25}$$

Where β is represent by equation (2.26) and, ϕ_Δ in expression (2.27) is the phase difference between $S(z)$ and $\hat{S}(z)$.

$$\beta = \mu A^2 A_s \tag{2.26}$$

$$\phi_\Delta = \phi_S - \phi_{\hat{S}} \tag{2.27}$$

A review of both equations (3.1) and (2.25) evidence that Transfer function of Adaptive Notch Filter utilizing Delayed FxLMS algorithm mainly depends of the characteristics of the system itself. Thus, in order to improve the performance of this algorithm is necessary to select the optimum value of step-size μ or minimize the differences between the secondary path transfer function $S(z)$ and its estimate $\widehat{S}(z)$.

Important constraints

According to [KM99] if β is small, the poles of $H(z)$ are complex conjugate with radius $r_p = \sqrt{1-\beta\cos(\phi_\Delta)}$. As it is showed in (2.26) β is positive, thus, the stability condition is (2.28).

$$\cos(\phi_\Delta) > 0 \; or \; -90^\circ < \phi_\Delta < 90^\circ \tag{2.28}$$

Additionally in [KM99] is given the time constant adaptation approximated in (2.29).

$$\tau_{mse} \leqslant \frac{2t_s}{\mu A^2} \tag{2.29}$$

Chapter 3

Optimization of Delayed FxLMS ANC

The present research has as objective the development of the optimization of the Delayed FxLMS algorithm, the justification of this selection is described in the following paragraphs.

As it is detailed in the last chapter, Delayed FxLMS algorithm focuses on Single Frequency ANC systems, which have the lowest order of adaptive filter of LMS algorithms. Low order filters imply low computational burden, thus less complex and expensive devices can support this ANC algorithm.

Single Frequency ANC systems in less complex devices would be the first step to less complex Multi-frequency ANC systems.

3.1 Analysis of Single Frequency ANC systems

3.1.1 Stability Conditions

The initial part of this sections is the analysis in Time Domain of the stability conditions for an Adaptive Notch Canceller or Single Frequency ANC system.

In order to achieve the mentioned purpose, it is used transfer function (3.1) of Kuo and Morgan.

$$H(z) = \frac{E(z)}{D(z)} = \frac{z^2 - 2z\cos(\omega_0) + 1}{z^2 - (2 - \mu A^2)z\cos(\omega_0) + 1 - \mu A^2} \tag{3.1}$$

However, Kuo and Morgan in [KM99] do not consider sampling time, transfer function (3.2) considers mentioned element in order to develop the corresponding analysis,

$$H(z) = \frac{E(z)}{D(z)} = \frac{z^2 - 2z\cos(\omega_0 t_s) + 1}{z^2 - (2 - \mu A^2)z\cos(\omega_0 t_s) + 1 - \mu A^2} \tag{3.2}$$

From transfer function (3.2), it is obtained expression (3.3) to represent its poles.

$$p = (1 - \frac{\mu A^2}{2})\cos(\omega_0 t_s) \pm \sqrt{(1 - \frac{\mu A^2}{2})^2 \cos^2(\omega_0 t_s) - (1 - \mu A^2)} \tag{3.3}$$

It is considered two cases, the first when the expression of the radical is imaginary and the second when it is real.

Case I: Complex poles

If the expression of the radical results an imaginary, it is obtained expression (3.4).

$$(1 - \frac{\mu A^2}{2})^2 \cos^2(\omega_0 t_s) - (1 - \mu A^2) < 0 \tag{3.4}$$

Considering system stability, according to (3.3) and (3.4), the condition of radius of the pole vector is expressed by equation (3.5).

$$r_p = \sqrt{1 - \mu A^2} \leqslant 1 \tag{3.5}$$

Thus, (3.6) represent interval for μ in order to keep stability.

$$\mu \in [0; \frac{1}{A^2}] \tag{3.6}$$

Additionally it is necessary analyzes the initial expression (3.4). It is expanded in expression (3.7).

$$(1 - \mu A^2)\cos^2(\omega_0 t_s) + \frac{\mu^2 A^2}{4}\cos^2(\omega_0 t_s) - (1 - \mu A^2) < 0 \tag{3.7}$$

Operating expression (3.7), it is obtained (3.8).

$$(\frac{\mu A^2}{2} + \tan^2(\omega_0 t_s) - \frac{\sin(\omega_0 t_s)}{\cos^2(\omega_0 t_s)})(\frac{\mu A^2}{2} + \tan^2(\omega_0 t_s) + \frac{\sin(\omega_0 t_s)}{\cos^2(\omega_0 t_s)}) < 0 \tag{3.8}$$

Analysing (3.8), it is obtained the operation interval for μ in (3.9)

$$\mu \in \langle \frac{2(-|\frac{\sin(\omega_0 t_s)}{\cos^2(\omega_0 t_s)}| - \tan^2(\omega_0 t_s))}{A^2}; \frac{2(|\frac{\sin(\omega_0 t_s)}{\cos^2(\omega_0 t_s)}| - \tan^2(\omega_0 t_s))}{A^2} \rangle \tag{3.9}$$

Therefore, for an imaginary radical it is obtained the following operation interval (3.10) for μ, from (3.6) and (3.9).

$$\mu \in [0; \frac{1}{A^2}] \cap \langle \frac{2(-|\frac{\sin(\omega_0 t_s)}{\cos^2(\omega_0 t_s)}| - \tan^2(\omega_0 t_s))}{A^2}; \frac{2(|\frac{\sin(\omega_0 t_s)}{\cos^2(\omega_0 t_s)}| - \tan^2(\omega_0 t_s))}{A^2} \rangle \quad (3.10)$$

Case II: Real poles

Another situation is obtained when radical expression is real, as is expressed by (3.11).

$$(1 - \frac{\mu A^2}{2})^2 \cos^2(\omega_0 t_s) - (1 - \mu A^2) \geqslant 0 \quad (3.11)$$

How is expected, expression (3.11) can be represented as (3.12), similar to (3.8).

$$(\frac{\mu A^2}{2} + \tan^2(\omega_0 t_s) - \frac{\sin(\omega_0 t_s)}{\cos^2(\omega_0 t_s)})(\frac{\mu A^2}{2} + \tan^2(\omega_0 t_s) + \frac{\sin(\omega_0 t_s)}{\cos^2(\omega_0 t_s)}) \geqslant 0 \quad (3.12)$$

Hence, first operation interval for μ is represented by (3.13).

$$\mu \in \langle -\infty; \frac{2(-|\frac{\sin(\omega_0 t_s)}{\cos^2(\omega_0 t_s)}| - \tan^2(\omega_0 t_s))}{A^2}] \cup [\frac{2(-|\frac{\sin(\omega_0 t_s)}{\cos^2(\omega_0 t_s)}| - \tan^2(\omega_0 t_s))}{A^2}; +\infty \rangle \quad (3.13)$$

Then, it is necessary to analyse the radius of the pole vector expressed by (3.14).

$$0 \leqslant \sqrt{[(1 - \frac{\mu A^2}{2}) \cos(\omega_0 t_s) \pm \sqrt{(1 - \frac{\mu A^2}{2})^2 \cos^2(\omega_0 t_s) - (1 - \mu A^2)}]^2} \leqslant 1 \quad (3.14)$$

As part of the analysis, first considers positive result of the radical, thus, is analysed the maximum value by (3.15).

$$(1 - \frac{\mu A^2}{2}) \cos(\omega_0 t_s) + \sqrt{(1 - \frac{\mu A^2}{2})^2 \cos^2(\omega_0 t_s) - (1 - \mu A^2)} \leqslant 1 \quad (3.15)$$

$$\sqrt{(1 - \frac{\mu A^2}{2})^2 \cos^2(\omega_0 t_s) - (1 - \mu A^2)} \leqslant 1 - (1 - \frac{\mu A^2}{2}) \cos(\omega_0 t_s) \quad (3.16)$$

The resulting expression is (3.16), where both parts are positives. Operating, it is obtained the expression (3.17)

$$\mu \leqslant \frac{2}{A^2} \quad (3.17)$$

As second part of analysis of (3.14), it is considered the minimum value for a negative result of the radical in (3.18). As is showed, this expression is always positive.

$$0 \leqslant \sqrt{[(1-\frac{\mu A^2}{2})\cos(\omega_0 t_s) - \sqrt{(1-\frac{\mu A^2}{2})^2\cos^2(\omega_0 t_s) - (1-\mu A^2)}]^2} \tag{3.18}$$

Therefore, the analysis of stability in this case for pole vector obtains the following operation interval for μ.

$$\mu \in [0; \frac{2}{A^2}] \tag{3.19}$$

Hence, Case II is resumed by (3.20) as operation interval for μ, considering expressions (3.13) and (3.19).

$$\mu \in [0; \frac{2}{A^2}] \cap \{\langle -\infty; \frac{2(-|\frac{\sin(\omega_0 t_s)}{\cos^2(\omega_0 t_s)}| - \tan^2(\omega_0 t_s))}{A^2}] \cup [\frac{2(|\frac{\sin(\omega_0 t_s)}{\cos^2(\omega_0 t_s)}| - \tan^2(\omega_0 t_s))}{A^2}; +\infty\rangle\} \tag{3.20}$$

Analysis of Intervals values

As a conclusion of Cases I and II, μ has the operation interval expressed in (3.10) or (3.20). Nonetheless, it is necessary analyzes the expressions composes by $\omega_0 t_s$, in order to obtain defined operation intervals of μ.

Considering (3.10) as (3.21) and (3.20) as (3.22), values of λ_1 and λ_2 are expressed in (3.23) and (3.24) respectively.

$$\mu \in [0; \frac{1}{A^2}] \cap \langle \frac{2\lambda_1}{A^2}; \frac{2\lambda_2}{A^2} \rangle \tag{3.21}$$

$$\mu \in [0; \frac{2}{A^2}] \cap \{\langle -\infty; \frac{2\lambda_1}{A^2}] \cup [\frac{2\lambda_2}{A^2}; +\infty\rangle\} \tag{3.22}$$

$$\lambda_1 = -|\frac{\sin(\omega_0 t_s)}{\cos^2(\omega_0 t_s)})| - \tan^2(\omega_0 t_s) \tag{3.23}$$

$$\lambda_2 = |\frac{\sin(\omega_0 t_s)}{\cos^2(\omega_0 t_s)}| - \tan^2(\omega_0 t_s) \tag{3.24}$$

Analysing (3.23) is determined (3.25).

$$\lambda_1 < 0 \tag{3.25}$$

Thus, expression (3.26).

$$\frac{2\lambda_1}{A^2} < 0 \tag{3.26}$$

Expression (3.26) is sufficiently to be located because the other points in the intervals are all positive.

Now, it is analysed λ_2 in (3.27) since (3.24).

$$\lambda_2 = |\frac{\sin(\omega_0 t_s)}{cos^2(\omega_0 t_s)}|(1 - |\sin(\omega_0 t_s)|) \tag{3.27}$$

Then, it is multiplied $(1 + |\sin(\omega_0 t_s)|)$ in numerator y denominator, it is obtained (3.28).

$$\lambda_2 = \frac{|\sin(\omega_0 t_s)|}{(1 + |\sin(\omega_0 t_s)|)} \tag{3.28}$$

Hence, is determined interval (3.29).

$$0 < \lambda_2 \leqslant \frac{1}{2} \tag{3.29}$$

Thus,

$$0 < \frac{2\lambda_2}{A^2} \leqslant \frac{1}{A^2} \tag{3.30}$$

Expression (3.30) is sufficiently because it is located between points 0 and $\frac{1}{A^2}$.

Finally, considering (3.26) and (3.30) in intervals (3.21) and (3.22), it is obtained the new intervals for μ expressed by (3.31) for complex poles and (3.32) for real poles.

$$\mu \in [0; \frac{2\lambda_2}{A^2}\rangle \tag{3.31}$$

$$\mu \in [\frac{2\lambda_2}{A^2}; \frac{2}{A^2}] \tag{3.32}$$

Joining both intervals, it is obtained the general interval of operation for μ in (3.33).

$$\mu \in [0; \frac{2}{A^2}] \tag{3.33}$$

3.1.2 Time Response

Considering the equations of Adaptive Notch Filters presented in the State of the Art.

$$w_0(n+1) = w_0(n) + \mu e(n) x_0(n) \tag{3.34}$$

$$w_1(n+1) = w_1(n) + \mu e(n) x_1(n) \tag{3.35}$$

$$y(n) = w_0(n) x_0(n) + w_1(n) x_1(n) \tag{3.36}$$

$$e(n) = d(n) - y(n) \tag{3.37}$$

Apparently a better convergence time can be achieved with the highest μ, according to (3.33) this would be $\frac{2}{A^2}$.

At this part it is analysed time response of the Adaptive Notch Filters (Single Frequency ANC systems) with different μ, and also is verified the stability interval obtained in the last part.

In the analysis, it is used a noise signal frequency of 60 Hz and sampling frequency of 2 kHz. These values are selected because ANC systems are designed to reduce low-frequency noise ($<$ 600 Hz) and considering the Nyquist Shannon sampling theorem the minimum sampling frequency for the maximum noise signal frequency should be 1.2 kHz.

Analysis of Time Response - Transfer Function

According to the reference signal expressed by (3.38), $A = 5$, $f_0 = 60$ and $t_s = 1/2000$.

$$x(n) = A \sin(\omega_0 n t_s) = A \sin(2\pi f_0 n t_s) \tag{3.38}$$

And the operation interval for μ is represented by (3.39)

$$\mu \in [0; \frac{2}{A^2}] = [0; 0.08] \tag{3.39}$$

Hence, values out of the interval become unstable the system. Fig. 3.1 shows the time response for $\mu = -0.001$ and $\mu = 0.081$.

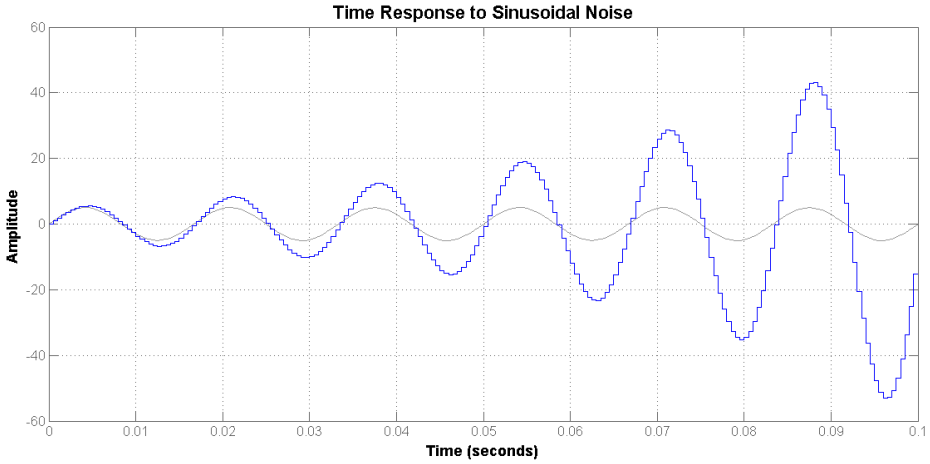

(a) Time Response for $\mu = -0.001$

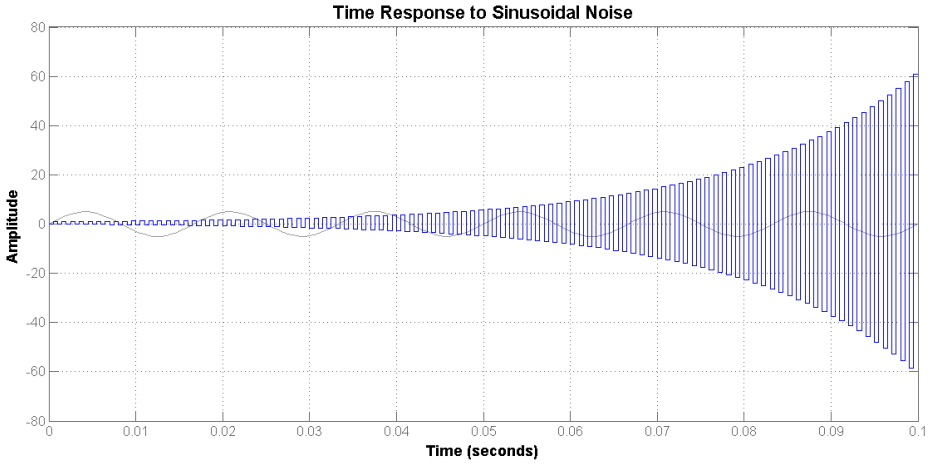

(b) Time Response for $\mu = 0.081$

Figure 3.1: Time responses for μ values out of the operation interval, gray line represents noise signal and blue line represents control signal

And values of the limits of the operation interval, become critically stable. Fig. 3.2 shows the time response for $\mu = 0$ and $\mu = 0.08$.

Considering that the operation interval of μ is the union of two operation intervals, one for complex poles and the other for real poles as is referenced by (3.31) and (3.32). The joining point is in $\mu = \frac{2\lambda_2}{A^2}$, considering (3.23) and the initial values of w_0 and t_s in the present subsection, it is obtained the value of the joining point in the expression (3.40).

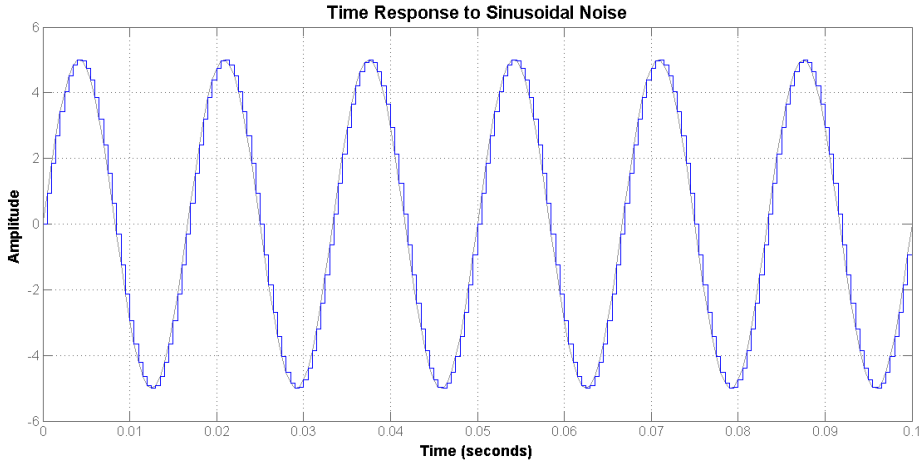

(a) Time Response for $\mu = 0$

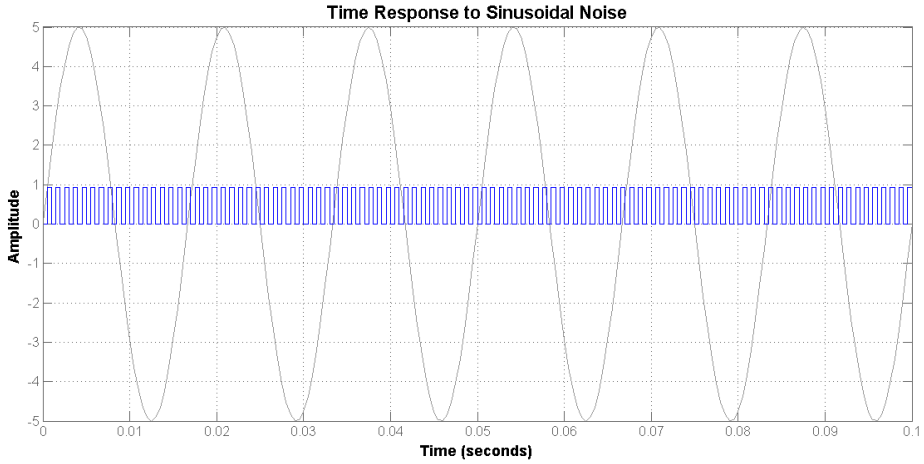

(b) Time Response for $\mu = 0.08$

Figure 3.2: Time responses for μ values in the limits of the operation interval, gray line represents noise signal and blue line represents control signal

$$\mu_{\lambda_2} = \frac{2|\sin(\omega_0 t_s)|}{A^2(1 + |\sin(\omega_0 t_s)|)} = 0.0126 \tag{3.40}$$

In Fig. 3.3 is showed the time response for μ in the joining point referenced by (3.40). Additionally is showed the time response for $\mu = \frac{1}{A^2}$, another important point in the operation intervals developed in this section and also the middle point of the operation interval analysed.

$$\mu_{mid} = \frac{1}{A^2} = 0.04 \tag{3.41}$$

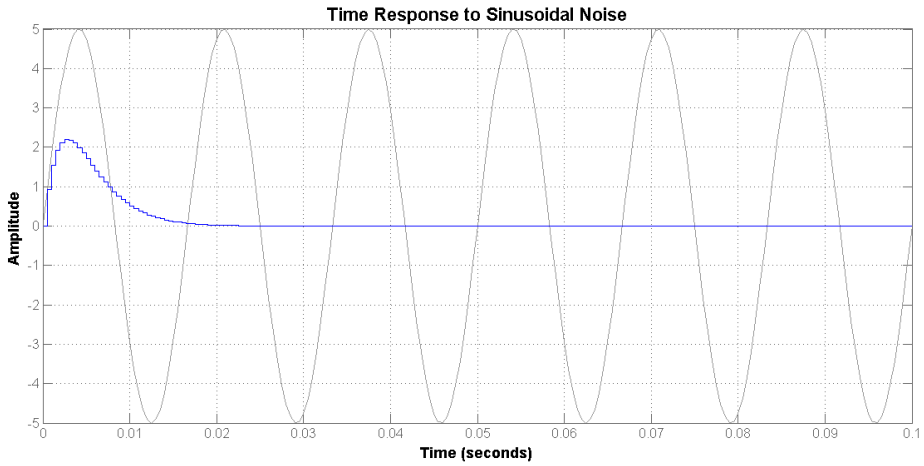

(a) Time Response for $\mu = \mu_{\lambda_2} = 0.0126$

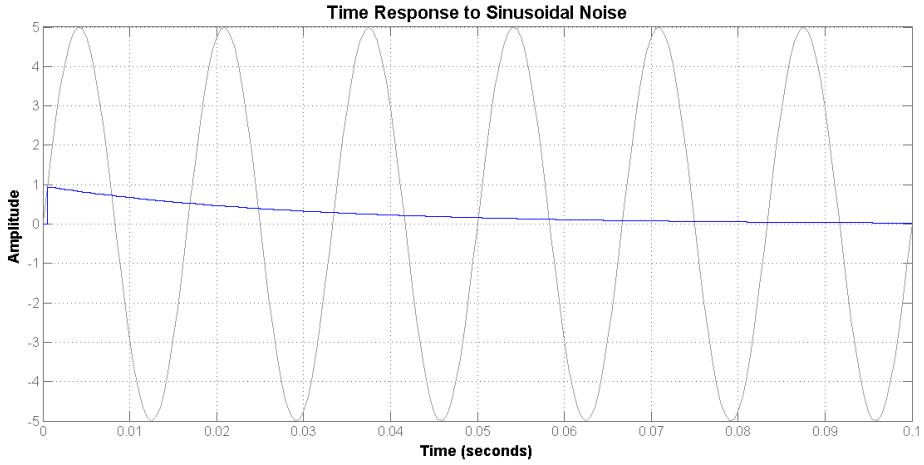

(b) Time Response for $\mu = \mu_{mid} = 0.04$

Figure 3.3: Time responses for μ values in important points of the operation interval, gray line represents noise signal and blue line represents control signal

As can be reviewed in Fig. 3.3, the time response for both points is good. Apparently μ_{λ_2} presents better stationary error and μ_{mid} better convergence. It is necessary a study of the convergence time in order to determine the best μ for the frequencies that are tested in the prototype of ANC system.

3.2 Optimal Step-Size μ_o

As previously observed, step-size μ values should be limited in order to maintain stability in Single-Frequency ANC systems. Additionally, this previous analysis evidences the relationship between the value of μ and Single-Frequency response.

In this subsection it is calculate de optimal step-size μ_o for the Single Frequecy ANC system in order to obtain the best settling time.

According to the settling time concept, it is determined by two different criteria.

With a criteria of 2% is expressed by equation (3.42).

$$t_{ss} = \frac{4}{\sigma} \tag{3.42}$$

With a criteria of 5% is expressed by equation (3.43).

$$t_{ss} = \frac{3}{\sigma} \tag{3.43}$$

Where σ is the real part of the dominant continuous pole showed in (3.44)

$$s = -\sigma \pm j\omega_d \tag{3.44}$$

And this continuous pole has its correspondent discrete pole, which is obtained through formula (3.45).

$$z = e^{t_s s} \tag{3.45}$$

Where the discrete pole z is denoted by expression (3.46).

$$z = c \pm jd \tag{3.46}$$

Considering equations (3.44) and (3.46), it is developed the expression (3.45).

$$c \pm jd = e^{-t_s\sigma}(\cos(\omega_d t_s) \pm j\sin(\omega_d t_s)) \tag{3.47}$$

Equations (3.48) and (3.49) are obtained from (3.45) considering that discrete poles are step-size μ functions.

$$c(\mu) = e^{-t_s\sigma}\cos(\omega_d t_s) \tag{3.48}$$

$$d(\mu) = e^{-t_s\sigma}\sin(\omega_d t_s) \tag{3.49}$$

Note that $c(\mu)$ and $d(\mu)$ have equal sign that $\cos(\omega_0 t_s)$ and $\sin(\omega_0 t_s)$ respectively. And from (3.48) and (3.49) it is obtained the expression (3.50).

$$\omega_d t_s = \arctan(\frac{d(\mu)}{c(\mu)}) \tag{3.50}$$

Consequently, can be obtained two possibles expressions (3.51) and (3.52) in order to determine the value of σ in function of the step-size μ.

$$\sigma(\mu) = -\frac{1}{t_s}\ln(\frac{c(\mu)}{\cos(\arctan(\frac{d(\mu)}{c(\mu)}))}) \tag{3.51}$$

$$\sigma(\mu) = -\frac{1}{t_s}\ln(\frac{d(\mu)}{\sin(\arctan(\frac{d(\mu)}{c(\mu)}))}) \tag{3.52}$$

According to (3.48) and (3.49), the expression that are into de natural logarithm in (3.51) and (3.52) always is a non-negative number, and the logarithm always have solution.

Hence, it is necessary to find the optimal value for the step-size μ_o in order to obtain the maximum value of σ thus the minimum settling time (according to (3.42) and (3.43)).

In this case the dominant discrete pole is representing by the expression (3.3), thus it is obtained the correspondence defined by (3.53).

$$c(\mu) \pm jd(\mu) = (1 - \frac{\mu A^2}{2})\cos(\omega_0 t_s) \pm \sqrt{(1 - \frac{\mu A^2}{2})^2\cos^2(\omega_0 t_s) - (1 - \mu A^2)} \tag{3.53}$$

Notwithstanding, there are two possibles cases. The following subsections detail this analysis.

3.2.1 Case I: Complex poles

The present case considers an imaginary solution for radical expression of equation (3.53), thus two complex poles with equal real part. Consequently, both poles are dominant, and real part is analysed indistinctly of the poles.

Another important consideration is that step-size μ is constrained by interval $[0, \frac{2\lambda_2}{A^2} >$ according to Stability Conditions. Hence, (3.53) in this part is represent by (3.54)

$$c(\mu) \pm jd(\mu) = (1 - \frac{\mu A^2}{2})\cos(\omega_0 t_s) \pm j\sqrt{(1-\mu A^2) - (1-\frac{\mu A^2}{2})^2\cos^2(\omega_0 t_s)} \quad (3.54)$$

Therefore, according to (3.51), $\sigma(\mu)$ is expressed by (3.55).

$$\sigma(\mu) = -\frac{1}{t_s}\ln(\frac{(1-\frac{\mu A^2}{2})\cos(\omega_0 t_s)}{\cos(\arctan(\frac{\pm\sqrt{(1-\mu A^2)-(1-\frac{\mu A^2}{2})^2\cos^2(\omega_0 t_s)}}{(1-\frac{\mu A^2}{2})\cos(\omega_0 t_s)}))} \quad (3.55)$$

The maximum value of σ will be achieved by an optimal value of μ (μ_o), for this value $\sigma'(\mu_o)$ should be zero. Therefore, it is derived the expression (3.55) to matching to zero, unfortunately (3.56) is obtained.

$$\sigma'(\mu) = \frac{A^2}{2t_s(1-\mu A^2)} \quad (3.56)$$

Expression (3.56) cannot be zero, thus function $\sigma(\mu)$ is an increasing or decreasing function in the interval $[0, \frac{2\lambda_2}{A^2}>$. In order to understand the behaviour (increasing or decreasing) of $\sigma(\mu)$, it is analysed its value for the critical values 0 and $\frac{2\lambda_2}{A^2}$.

For $\mu = 0$:

$$c(0) = (1 - \frac{(0)A^2}{2})\cos(\omega_0 t_s) = \cos(\omega_0 t_s) \quad (3.57)$$

$$d(0) = \sqrt{(1-(0)A^2) - (1-\frac{(0)A^2}{2})^2\cos^2(\omega_0 t_s)} = \pm\sin(\omega_0 t_s) \quad (3.58)$$

Thus,

$$\sigma(0) = -\frac{1}{t_s}\ln(\frac{\cos(\omega_0 t_s)}{\cos(\arctan(\frac{\pm\sin(\omega_0 t_s)}{\cos(\omega_0 t_s)}))}) = 0 \quad (3.59)$$

First Result: $\sigma(0) = 0$;

For $\mu = \mu_{\lambda_2} = \frac{2\lambda_2}{A^2}$:
According to expression (3.28) $\lambda_2 = \frac{|\sin(\omega_0 t_s)|}{1+|\sin(\omega_0 t_s)|}$:

$$c(\mu_{\lambda_2}) = \frac{\cos(\omega_0 t_s)}{1+|\sin(\omega_0 t_s)|} \quad (3.60)$$

$$d(\mu_{\lambda_2}) = 0 \quad (3.61)$$

Considering that the expression into the natural logarithm is always positive (as it is noted before).

$$0 \leqslant \frac{c(\mu_{\lambda_2})}{\cos(\arctan(\frac{0}{c(\mu_{\lambda_2})}))} \leqslant 1 \tag{3.62}$$

Thus,

$$\sigma(\mu_{\lambda_2}) = -\frac{1}{t_s}\ln(\frac{c(\mu_{\lambda_2})}{\cos(\arctan(\frac{0}{c(\mu_{\lambda_2})}))} > 0 \tag{3.63}$$

Second Result: $\sigma(\mu_{\lambda_2}) > 0$

Considering that $\mu_{\lambda_2} > 0$, $\sigma(\mu_{\lambda_2}) > \sigma(0)$ and $\sigma'(\mu) \neq 0$ for the interval $[0, \mu_{\lambda_2} >$. The conclusion is that $\sigma(\mu)$ is an increasing function for this interval.

3.2.2 Case II: Real Poles

In this case, there are 2 real poles, one of them is the dominant pole, according to the Stability Conditions, the step-size μ is constrained by the interval $[\frac{2\lambda_2}{A^2}, \frac{2}{A^2}]$. And the expression for the real part $c(u)$ is represented by (3.64).

$$c(u) = (1 - \frac{\mu A^2}{2})\cos(\omega_0 t_s) \pm \sqrt{(1 - \frac{\mu A^2}{2})^2\cos^2(\omega_0 t_s) - (1 - \mu A^2)} \tag{3.64}$$

Expression (3.51) is reduced in (3.65). (according the observation of the value into the natural logarithm)

$$\sigma(\mu) = -\frac{1}{t_s}\ln(|c(u)|) \tag{3.65}$$

Considering the two real poles as $\sigma_1(\mu)$ and $\sigma_2(\mu)$, where $\sigma_1(\mu) \leqslant \sigma_2(\mu)$.

Obviously $\sigma_1(\mu)$ should be the dominant pole and according to (3.65) it is obtained that $c_1(\mu) \geqslant c_2(\mu)$, where $c_1(\mu)$ and $c_2(\mu)$ are the corresponding discrete poles for $\sigma_1(\mu)$ and $\sigma_2(\mu)$ respectively.

According to $c_1(\mu) \geqslant c_2(\mu)$, it is obtained the expressions (3.66) and (3.67).

$$c_1(\mu) = (1 - \frac{\mu A^2}{2})\cos(\omega_0 t_s) + \sqrt{(1 - \frac{\mu A^2}{2})^2\cos^2(\omega_0 t_s) - (1 - \mu A^2)} \tag{3.66}$$

$$c_2(\mu) = (1 - \frac{\mu A^2}{2})\cos(\omega_0 t_s) - \sqrt{(1 - \frac{\mu A^2}{2})^2\cos^2(\omega_0 t_s) - (1 - \mu A^2)} \tag{3.67}$$

As $\sigma_1(\mu)$ is the dominant pole, thus $c_1(\mu)$ would be the discrete dominant pole. Finally it is determined the expression (3.68).

$$\sigma(\mu) = -\frac{1}{t_s}\ln((1-\frac{\mu A^2}{2})\cos(\omega_0 t_s) + \sqrt{(1-\frac{\mu A^2}{2})^2\cos^2(\omega_0 t_s) - (1-\mu A^2)}) \quad (3.68)$$

In order to find the optimal value of μ (μ_o) to obtain the maximum value of σ it is analysed the value of $\sigma'(\mu)$ in (3.69), besides $\sigma'(\mu_o)$ should be zero.

$$\sigma'(\mu) = \frac{A^2\sin^2(\omega_0 t_s)}{2t_s\Delta(\mu)(\frac{\mu A^2\cos(\omega_0 t_s)}{2} - 1)} \quad (3.69)$$

Where $\Delta(\mu)$ is expressed by (3.70).

$$\Delta(\mu) = \sqrt{(1-\frac{\mu A^2}{2})^2\cos^2(\omega_0 t_s) - (1-\mu A^2)} \quad (3.70)$$

Expression (3.69) cannot be zero for any value of μ, thus $\sigma'(\mu)$ is an increasing or decreasing function in the interval $[\frac{2\lambda_2}{A^2}, \frac{2}{A^2}]$. At the same way, $\sigma(\mu)$ is evaluated for the critical values $\frac{2\lambda_2}{A^2}$ and $\frac{2}{A^2}$, in order to know if it is a increasing or decreasing function for the mentioned interval.

For $\mu = \mu_{\lambda_2} = \frac{2\lambda_2}{A^2}$:

According to (3.28) $\lambda_2 = \frac{|\sin(\omega_0 t_s)|}{1+|\sin(\omega_0 t_s)|}$:

$$c(\mu_{\lambda_2}) = \frac{\cos(\omega_0 t_s)}{1+|\sin(\omega_0 t_s)|} \quad (3.71)$$

Thus,

$$\sigma(\mu_{\lambda_2}) = -\frac{1}{t_s}\ln(|c(\mu_{\lambda_2})|) > 0 \quad (3.72)$$

First Result: $\sigma(\mu_{\lambda_2}) > 0$

For $\mu = \frac{2}{A^2}$:

$$c(\frac{2}{A^2}) = (1-1)\cos(\omega_0 t_s) + \sqrt{(1-1)^2\cos^2(\omega_0 t_s) - (1-2)} = 1 \quad (3.73)$$

Thus,

$$\sigma(\mu) = -\frac{1}{t_s}\ln(1) = 0 \tag{3.74}$$

Second Result: $\sigma(\frac{2}{A^2}) = 0$

Considering for the two results that $\mu_{\lambda_2} > \frac{2}{A^2}$, $\sigma(\mu_{\lambda_2}) < \sigma(\frac{2}{A^2})$ and $\sigma'(\mu) \neq 0$ for the interval $[\mu_{\lambda_2}, \frac{2}{A^2}]$. The conclusion is that $\sigma(\mu)$ is an decreasing function for this interval.

Furthermore, It is found that the $\sigma(\mu_{\lambda_2})$ for the interval $[0, \mu_{\lambda_2} >$ and for the interval $[\mu_{\lambda_2}, \frac{2}{A^2}]$ are the same, as it can be verified by the expressions (3.63) and (3.71).

3.2.3 Conclusion and Analysis

Finally, considering that the function $\sigma(\mu)$ is an increasing function in the interval $[0, \mu_{\lambda_2} >$, a decreasing function in the interval $[\mu_{\lambda_2}, \frac{2}{A^2}]$ and exist a common point in $\mu = \mu_{\lambda_2}$, the conclusion is that $\sigma(\mu)$ presents its maximum value when $\mu = \mu_{\lambda_2}$. Therefore μ_{λ_2} is the optimum value of step-size μ for the Single Frequency ANC system, as it is expressed by (3.75).

$$\mu_o = \mu_{\lambda_2} = \frac{2\lambda_2}{A^2} \tag{3.75}$$

In order to analyse the optimal step-size μ_o expression obtained in (3.75), it is evaluated the time response for the Single Frequency ANC system considering the optimal step-size $\mu_o = \mu_{\lambda_2}$ and with the following characteristics.

- Reference Signal Amplitude = 5 (no units).
- Reference Signal Frequency = 50 Hz.
- Sampling Frequency = 1 kHz.

This evaluation is resumed by Fig. 3.4, where time response obtained by the optimal step-size μ_o is compared with another time responses for different values of μ.

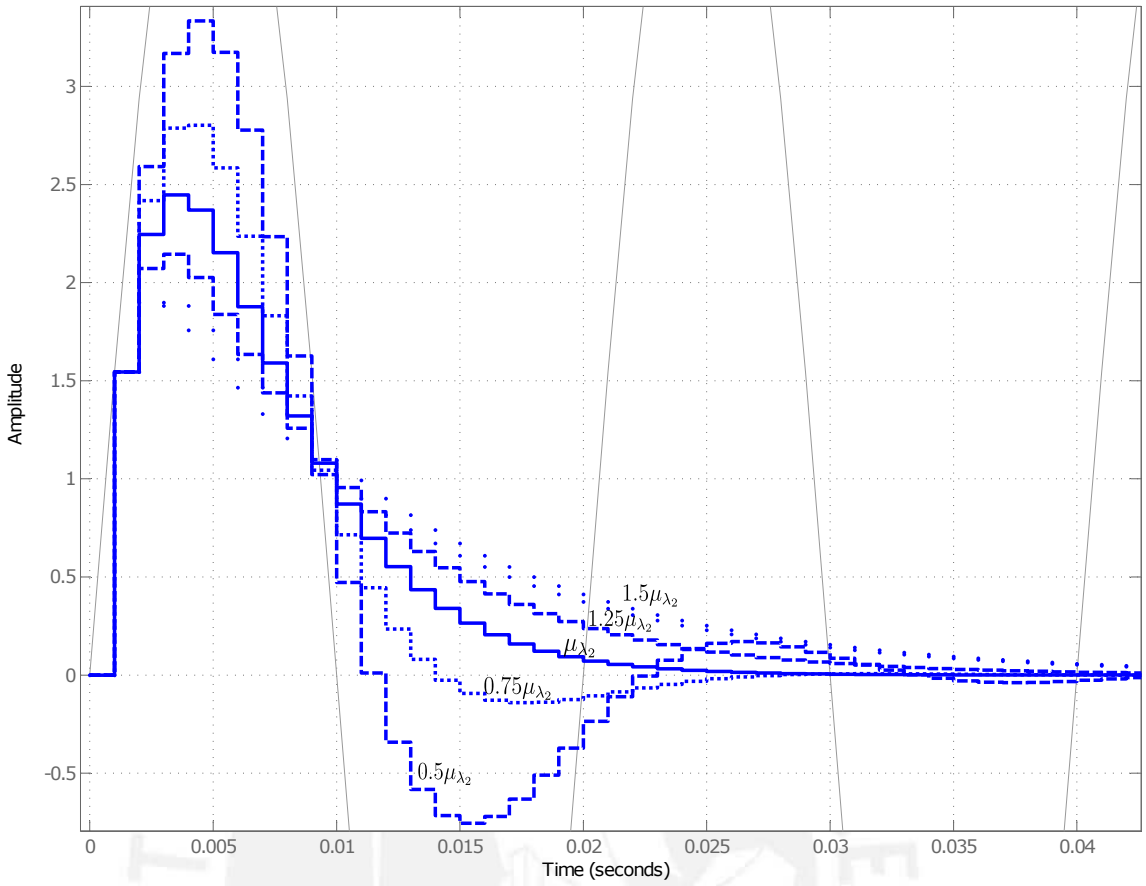

Figure 3.4: Transfer Function Response for $\mu = 0.5\mu_{\lambda_2}$, $0.75\mu_{\lambda_2}$, μ_{λ_2}, $1.25\mu_{\lambda_2}$ and $1.5\mu_{\lambda_2}$

Analysing Fig. 3.4, $\mu = \mu_o = \mu_{\lambda_2}$ presents a good time response, the same case occur with $\mu = 0.75\mu_{\lambda_2}$. The behaviour of all time responses implies that all the interval between the two mentioned values of μ present a good response and also values close to this range. Therefore, theoretical optimal step-size is really close to empirical, considering the empirical optimal step-size represent by expression (3.76).

$$\mu_o \in [0.75\mu_{\lambda_2}; \mu_{\lambda_2}] \tag{3.76}$$

3.2.4 Frequency Response Analysis

Additionally it is verified the behaviour of the system in the frequency domain, to achieve this purpose the Single Frequency ANC system is analysed by the Bode Diagram in magnitude and phase for the same values of step-size μ evaluated in time response.

Fig, 3.5 shows great similitude between the behaviour of the system for different values of μ, and the narrowness of the response in the frequency corresponding to

the reference noise signal, according to angular frequency relationship $\omega_0 = 2\pi f_0$.

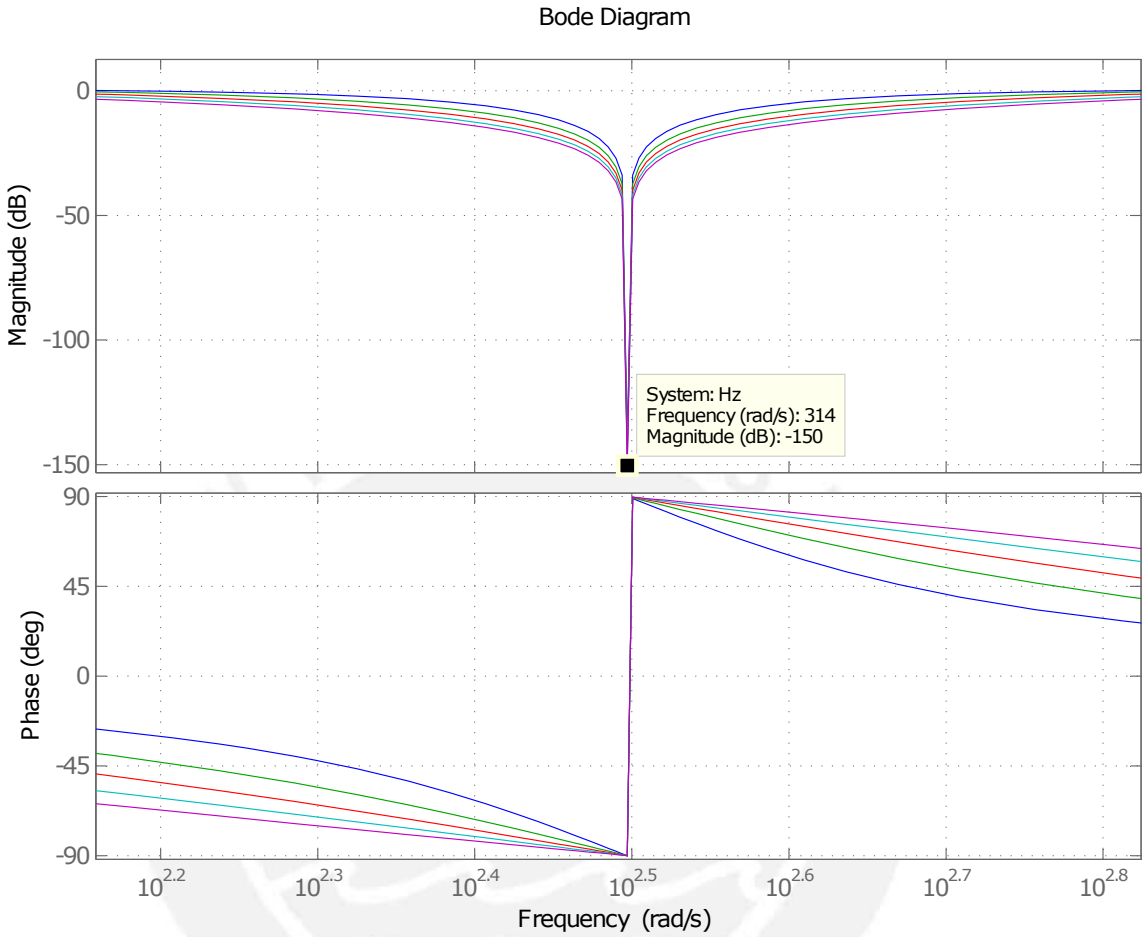

Figure 3.5: Bode Diagram considering $\mu = 0.5\mu_{\lambda_2}$, $0.75\mu_{\lambda_2}$, μ_{λ_2}, $1.25\mu_{\lambda_2}$ and $1.5\mu_{\lambda_2}$

This analysis reflects the weak impact of the variation of the step-size μ in the frequency response of a Single Frequency ANC system. Obviously, considering μ in its stability interval of operation.

3.3 Delayed FxLMS ANC Algorithm using Optimal Step-Size μ

Finally, the algorithm used in the Prototype of ANC system is the Delayed FxLMS algorithm, obviously for a single frequency noise signal as reference. Fig. 3.6 shows the structure of the algorithm.

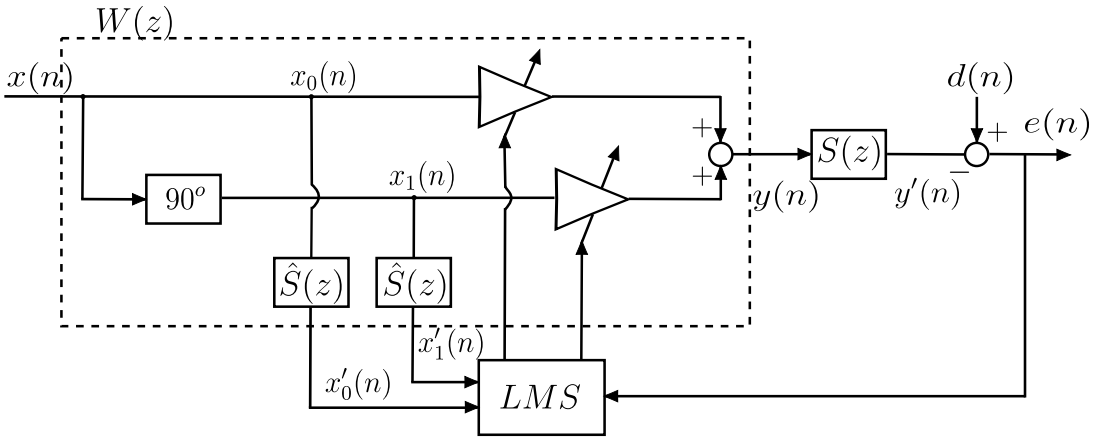

Figure 3.6: Delayed FxLMS ANC.
Source: [KM99]

As it is detailed in the last part of the state of the art, secondary path effect is balanced with the secondary path estimation, the results $x'_0(n)$ and $x'_1(n)$ are operated by the algorithm according to the equations (3.77) and (3.78).

$$x'_0(n) = A_s x_0(n - \Delta) \tag{3.77}$$

$$x'_1(n) = A_s x_1(n - \Delta) \tag{3.78}$$

Where A_s and Δ represents the amplitude and delay obtained of the secondary path obtained from secondary path estimation, step which should be realized before the beginning of the algorithm.

The LMS block is detailed by the equations (3.79), (3.80), (3.81) and (3.82), which have been mentioned before in the present document.

$$w_0(n+1) = w_0(n) + \mu e(n) x'_0(n) \tag{3.79}$$

$$w_1(n+1) = w_1(n) + \mu e(n) x'_1(n) \tag{3.80}$$

$$y(n) = w_0(n) x'_0(n) + w_1(n) x'_1(n) \tag{3.81}$$

$$e(n) = d(n) - y(n) \tag{3.82}$$

Additionally in the present research is added the calculus of the theoretical optimal step-size μ_o through the equations (3.83) and (3.84) obtaining (3.85) as final expression.

$$\mu_o = \mu_{\lambda_2} = \frac{2\lambda_2}{A^2} \tag{3.83}$$

$$\lambda_2 = \frac{|\sin(\omega_0 t_s)|}{1 + |\sin(\omega_0 t_s)|} \tag{3.84}$$

$$\mu_o = \frac{2|\sin(\omega_0 t_s)|}{A^2(1 + |\sin(\omega_0 t_s)|)} \tag{3.85}$$

As can be observed, calculus of optimal step-size should be initial, considering the frequency and amplitude of the single frequency noise signal obtained by the reference sensor and sampling time used by the controller.

Chapter 4
Simulations and Experimental Results

4.1 Simulations

In the present section is performed the simulation of the Delayed FxLMS ANC algorithm for a specific reference noise signal in order to identify the behaviour of the algorithm for different values of step-size μ, specially the optimal that is calculated before the operation of the algorithm. Bellow are described the characteristics used by these simulations.

- Reference Signal Amplitude = 512 (no units).
- Reference Signal Frequency = 50 Hz.
- Sampling Frequency = 1 kHz.

The figures obtained by simulation in the present section focus specially the evolution of the control signal and the residual error at the time in comparison with the reference noise signal. An important observation is that control signal is referenced to $y(n)$, thus it should be the most similar possible to the noise signal $d(n)$ in order to $e(n) = d(n) - y(n)$ tends to zero.

4.1.1 Simulation for the Optimal step-size μ

Considering the characteristics mentioned at the first part of the present subsection. It is obtained the value of the optimal step-size μ_o , detailed in the expression (4.1).

$$\mu_o = 1.8 \times 10^{-6} \tag{4.1}$$

Fig. 4.1a shows the behaviour of the control signal in order to track the noise signal. Additionally Fig. 4.1b presents the residual error obtained of the difference between the mentioned signals before.

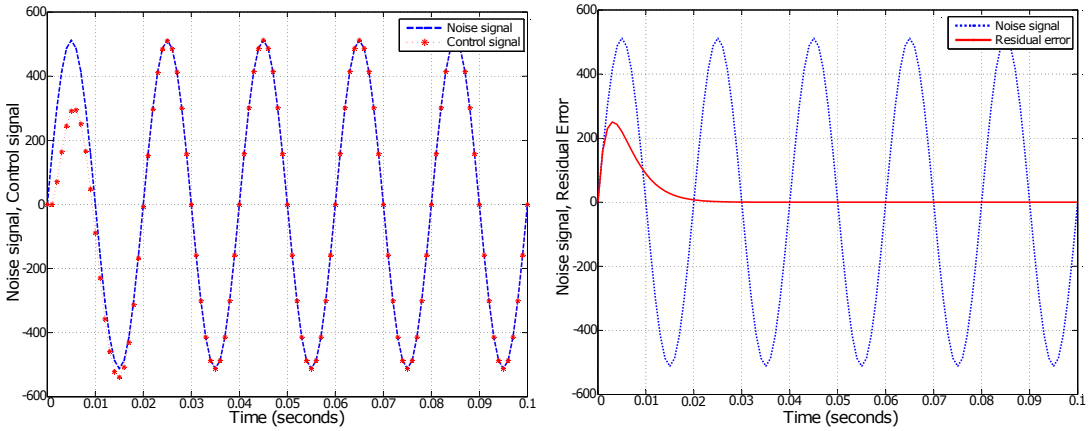

(a) Control signal for $\mu = \mu_o$

(b) Residual Error for $\mu = \mu_o$

Figure 4.1: Algorithm simulation for $\mu = \mu_o$

4.1.2 Simulations for critical values of μ

According to the stability conditions evaluated in the present document, there are two critical values for μ, the maximum and minimum of the operation interval referenced in (4.2).

$$\mu \in [0; \frac{2}{A^2}] \tag{4.2}$$

The minimum value of μ is represented by μ_L and the maximum by μ_H, its values are denoted by the expressions (4.3) and (4.4) respectively.

$$\mu = \mu_L = 0 \tag{4.3}$$

$$\mu = \mu_H = \frac{2}{A^2} = 7.6 \times 10^{-6} \tag{4.4}$$

Control signal and Residual Error signals for the minimum step-size μ_L are showed in Figs. 4.2a and 4.2b respectively, where it is noted a non-existent reduction of noise because the residual noise is the same that noise signal. However, the system does not show unstable characteristics.

Another undesirable result is obtained for the maximum step-size μ_H , control signal of Fig. 4.2c tracks noise signal but with important error that is showed by the residual error in Fig. 4.2d. It is not the same noise signal, but there is a constant noise with different amplitude and frequency of the reference.

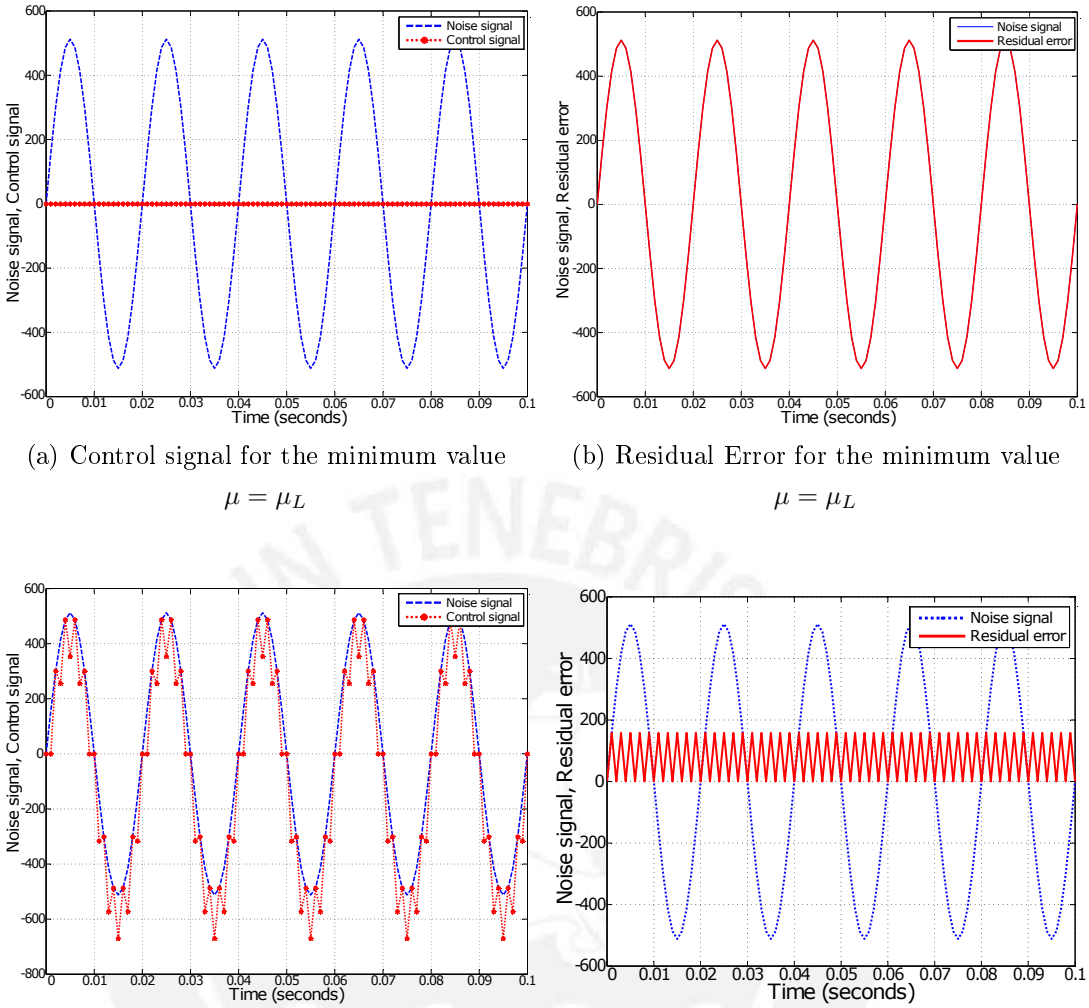

(a) Control signal for the minimum value $\mu = \mu_L$

(b) Residual Error for the minimum value $\mu = \mu_L$

(c) Control signal for the maximum value $\mu = \mu_H$

(d) Residual Error for the maximum value $\mu = \mu_H$

Figure 4.2: Simulation for the critical values $\mu = \mu_L$ and $\mu = \mu_H$

4.1.3 Simulations for higher μ values than the optimal

In order to verify the behaviour of the system for higher values of μ than the optimal μ_o, it is analysed two cases for specific values of μ detailed by equations (4.5) and (4.6).

$$\mu_+ = 2\mu_o = 3.6 \times 10^{-6} \tag{4.5}$$

$$\mu_{++} = 4\mu_o = 7.2 \times 10^{-6} \tag{4.6}$$

Figs. 4.3a and 4.3c reveals a faster response of the system with some overshoots

in comparison with the optimal step-size. However, Figs. 4.3b and 4.3d shows an increase of the residual error in the stationary time.

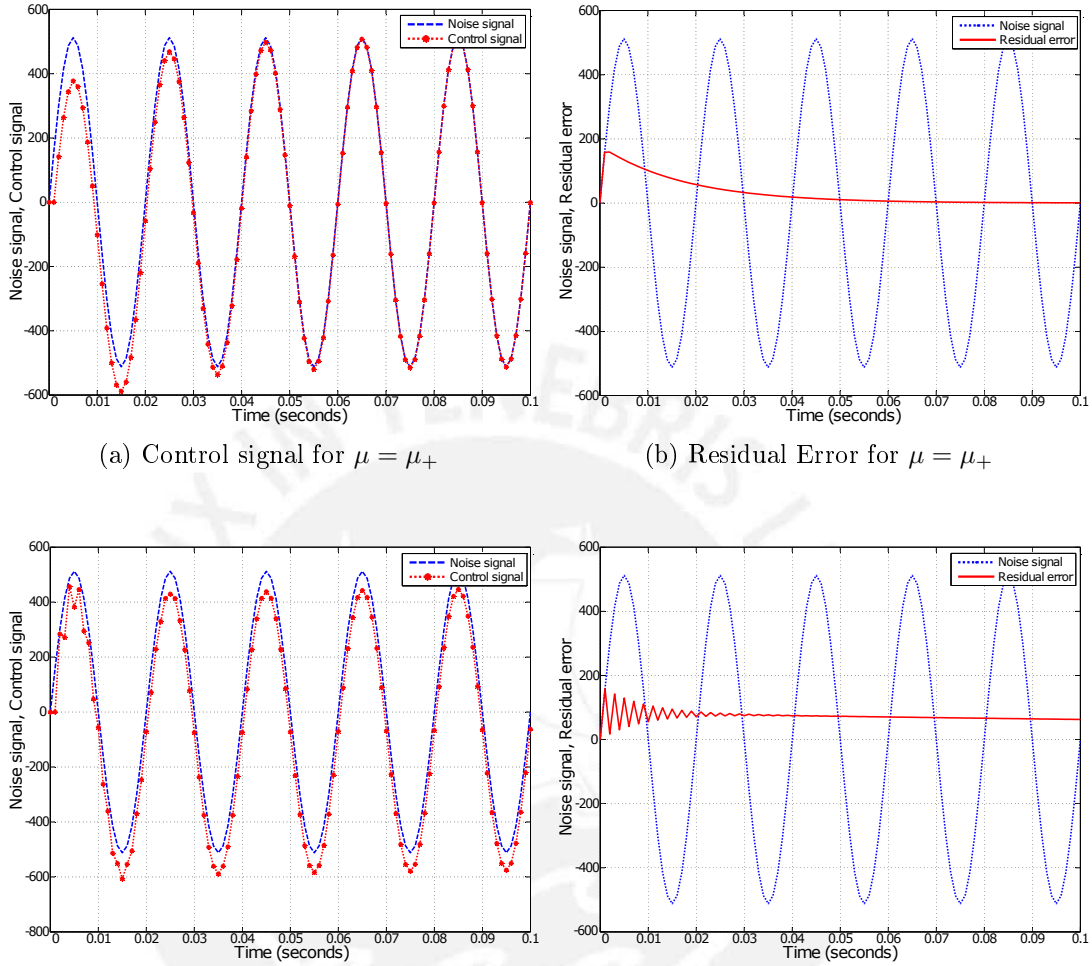

(a) Control signal for $\mu = \mu_+$

(b) Residual Error for $\mu = \mu_+$

(c) Control signal for $\mu = \mu_{++}$

(d) Residual Error for $\mu = \mu_{++}$

Figure 4.3: Simulation for higher μ values than the optimal

4.1.4 Simulations for lower μ values than the optimal

At the same way, this subsection verifies the response of the system for step-size values lower than the optimal μ_o, expressions (4.7) and (4.8) detail the chosen values for these simulations.

$$\mu_- = 5 \times 10^{-1} \mu_o = 0.9 \times 10^{-6} \tag{4.7}$$

$$\mu_{--} = 2.5 \times 10^{-1} \mu_o = 4.5 \times 10^{-7} \tag{4.8}$$

According with the theory, the behaviour of the control signal detailed by Figs. 4.4a and 4.4b shows that lower values than μ present slower response and Figs. 4.4c and 4.4d reflects an increase in the settling time.

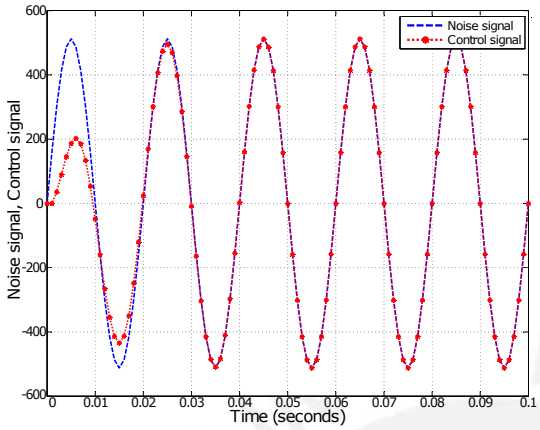

(a) Control signal for $\mu = \mu_-$

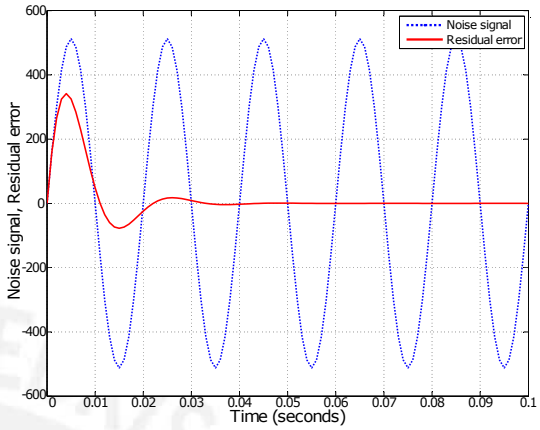

(b) Residual Error for $\mu = \mu_-$

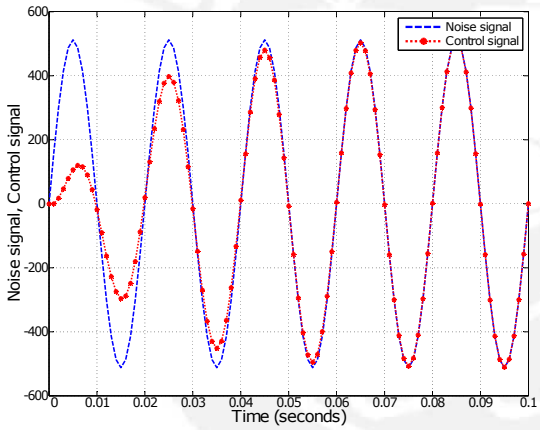

(c) Control signal for $\mu = \mu_{--}$

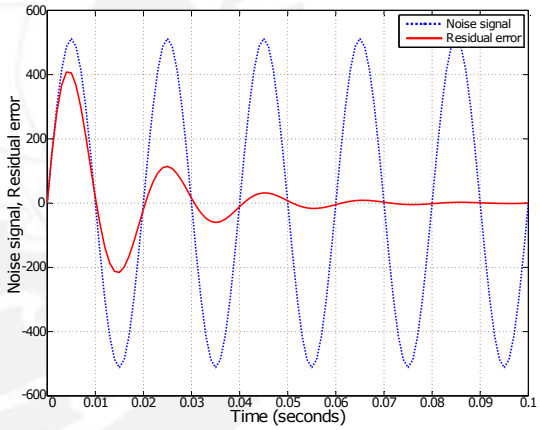

(d) Residual Error for $\mu = \mu_{--}$

Figure 4.4: Simulation for lower μ values than the optimal

4.2 Experimental Results

The present section aims to analyse the experimental results obtained from the evaluation of the Delayed FxLMS algorithm in a prototype of ANC system. All of this considering the optimal step-size μ.

4.2.1 Prototype of ANC system

In order to experiment the behaviour of a Single Frequency ANC system it is prepared a prototype of ANC system based in the module, which was designed and implemented by Jesús Alan Calderón Chavarri. The outside of the protoype is showed in Fig. 4.5, it consisted in a box isolated from external noise using insulation materials around itself.

Figure 4.5: Outside of the ANC system prototype

The final prototype, which was used in the experiments, is showed in Fig. 4.6 here the Loudspeaker 1 delivers noisy signal inside the box, microphone 1 measures this noisy signal, loudspeaker 2 delivers anti noise signal in order to attenuate it, and the error noise cancellation signal is measured by microphone 2.

Figure 4.6: Interior of the ANC system prototype

Delayed FxLMS algorithm and Optimal step-size calculus were implemented in an

ARDUINO UNO, which was used as controller for the experiments in the Single Frequency ANC system prototype. The complete scheme employed by the experiments considers three regions: acoustic, analogue and digital, Fig. 4.7 describes regions with all the blocks which have been considered.

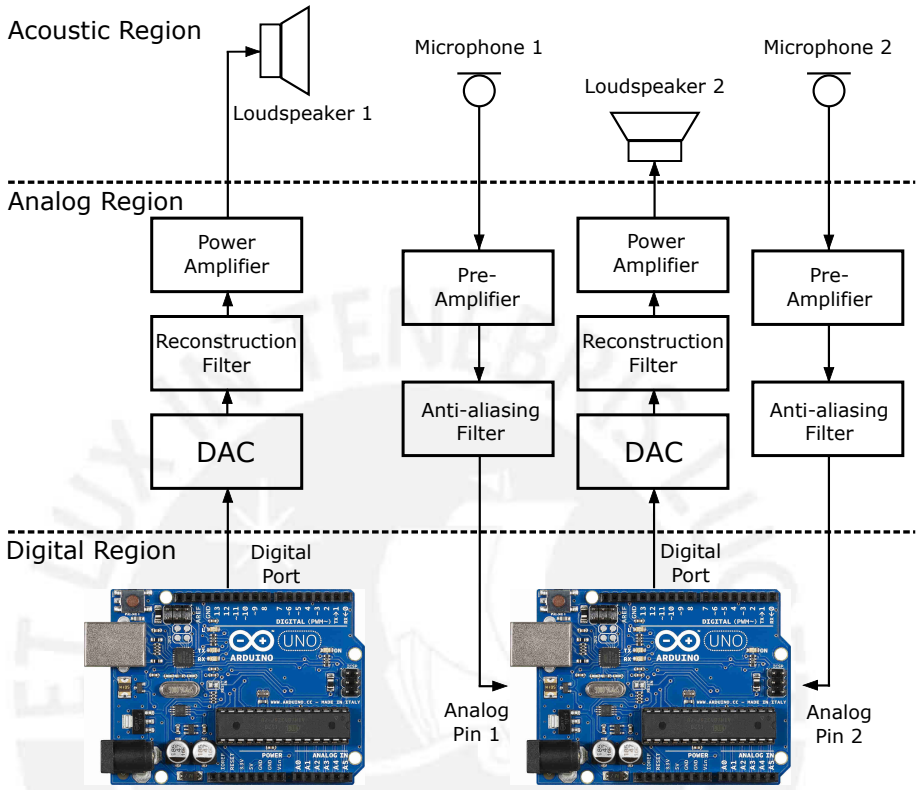

Figure 4.7: Scheme used by the Experiments

Additionally, it is important to explain that considerations of experiments are the same as simulations. As is detailed by the following list.

- Reference Signal Amplitude = 512 (no units).
- Reference Signal Frequency = 50 Hz.
- Sampling Frequency = 1 kHz.

Therefore, it is obtained the same value of optimal step-size described by (4.1). However, in contrast of simulations, figures of experiments consider as control signal the exact signal that is transmitted to the loudspeaker (anti-noise signal).

4.2.2 Experimental Results for the Optimal step-size μ_o and another μ values

As it is previously affirmed optimal step-size is where $\mu_o = 1.8 \times 10^{-6}$. Then, Figs. 4.8a and 4.8b shows the control signal and residual error response. An important detail observed in Fig. 4.8b is the presence of peaks in the residual error signal, the main reason of this type of irregularities is the presence of a little delay between noise and control signal, which suggests that the secondary path estimate $\widehat{S}(z)$ can present a little error or sampling/control frequency is too big in order to approximate the exact delay of $S(z)$.

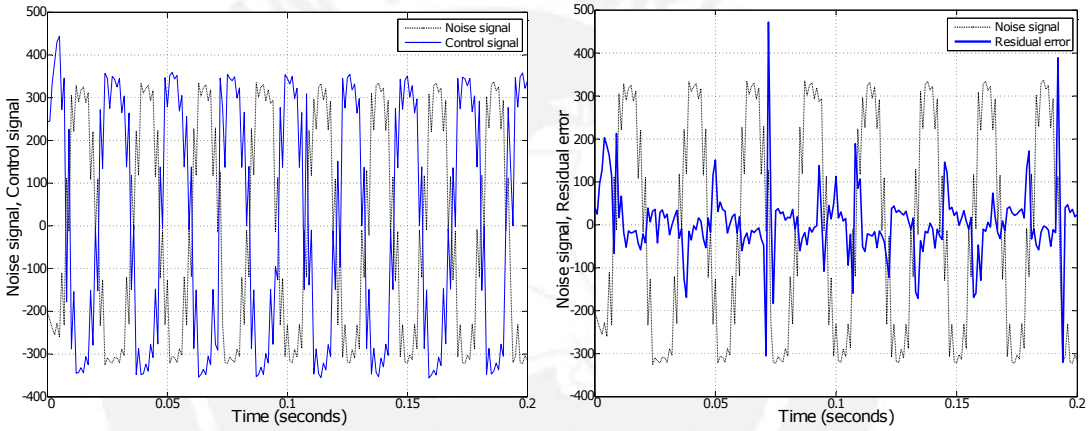

(a) Control signal for $\mu = \mu_o$ (b) Residual Error for $\mu = \mu_o$

Figure 4.8: Experimental results for $\mu = \mu_o$

Figures on the left side presents control signal in blue and also figures on the right side for the residual error. For all the figures noise reference signal is in gray color.

Results for higher values than μ_o

At the same way of Simulations, Fig. 4.9 presents results for higher values than μ_o. Values expressed by equations (4.9) and (4.10).

$$\mu_+ = 2\mu_o = 3.6 \times 10^{-6} \tag{4.9}$$

$$\mu_{++} = 4\mu_o = 7.2 \times 10^{-6} \tag{4.10}$$

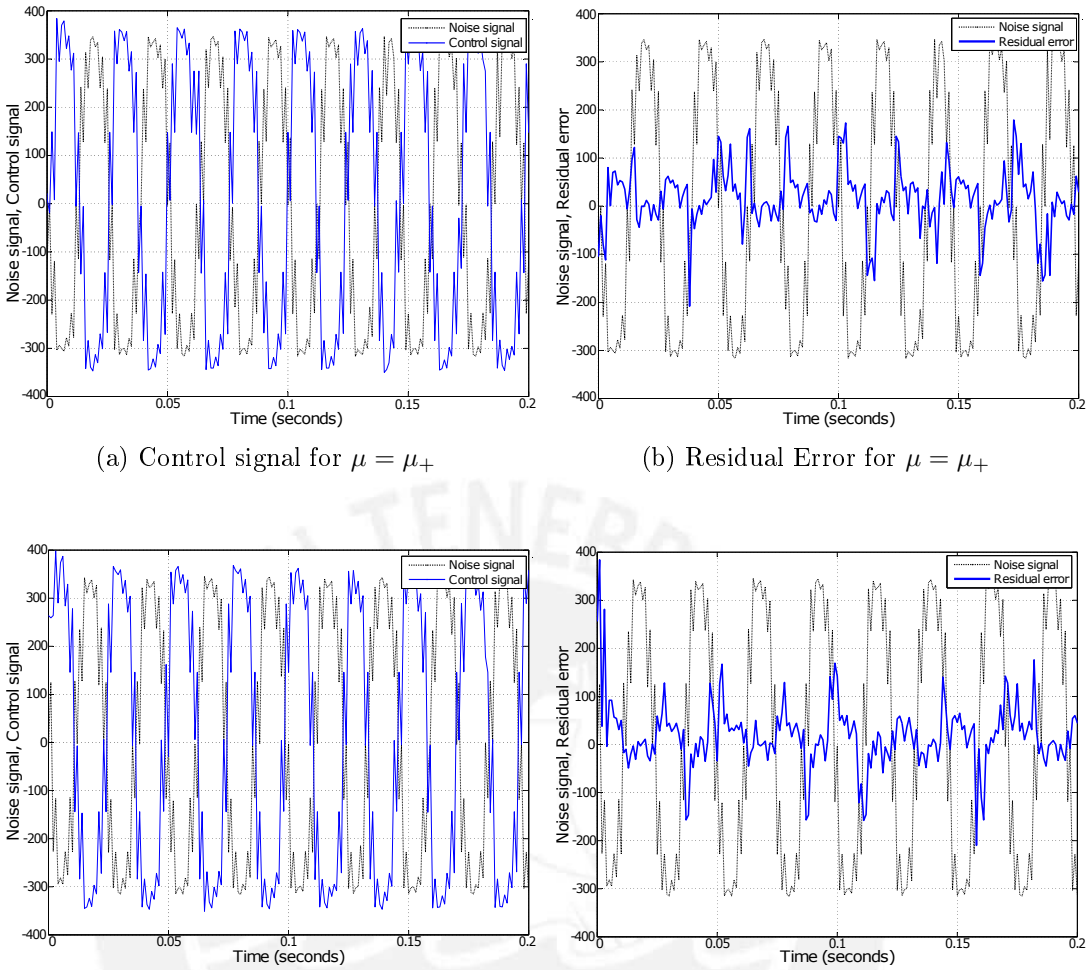

(a) Control signal for $\mu = \mu_+$

(b) Residual Error for $\mu = \mu_+$

(c) Control signal for $\mu = \mu_{++}$

(d) Residual Error for $\mu = \mu_{++}$

Figure 4.9: Results for higher values than μ_o

Results for lower values than μ_o

In this case Fig. 4.10 shows results for lower values than the optimal. This values are detailed by expressions (4.11) and (4.12).

$$\mu_- = 5 \times 10^{-1}\mu_o = 9 \times 10^{-7} \tag{4.11}$$

$$\mu_{--} = 2.5 \times 10^{-1}\mu_o = 4.5 \times 10^{-7} \tag{4.12}$$

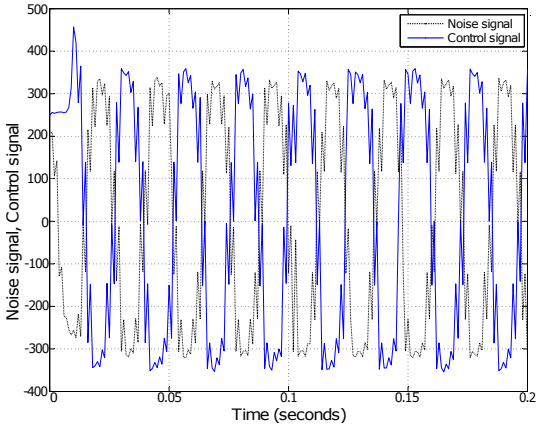

(a) Control signal for $\mu = \mu_-$

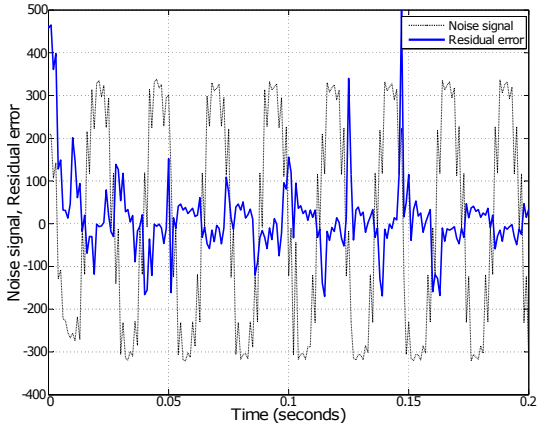

(b) Residual Error for $\mu = \mu_-$

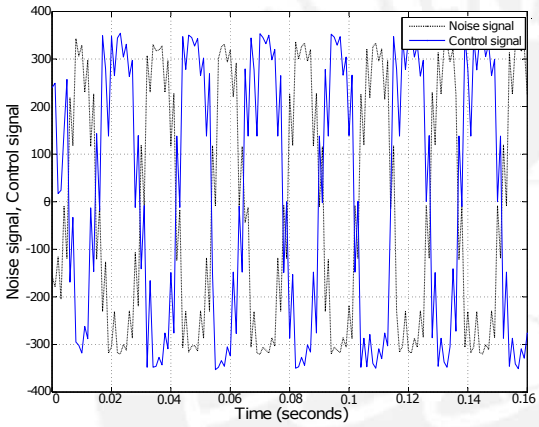

(c) Control signal for $\mu = \mu_{--}$

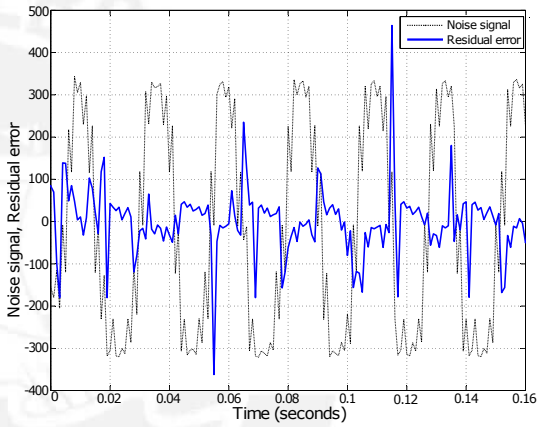

(d) Residual Error for $\mu = \mu_{--}$

Figure 4.10: Results for lower values than μ_o

Results for additional values of μ

Figures that present results for μ values different of the optimal μ_o do not show a clear behaviour of the system. is for that reason that experiments continues with lower values than previous, in order to increase the settling time and observe a slow behaviour of the system (easy to analyse). Chosen values are detailed by expressions (4.13), (4.14) and (4.15) and figures are grouped in Fig. 4.11.

$$\mu_a = 7.8125 \times 10^{-3}\mu_o = 1.406 \times 10^{-8} \tag{4.13}$$

$$\mu_b = 9.765 \times 10^{-4}\mu_o = 1.758 \times 10^{-9} \tag{4.14}$$

$$\mu_c = 6.1035 \times 10^{-5}\mu_o = 1.1 \times 10^{-10} \tag{4.15}$$

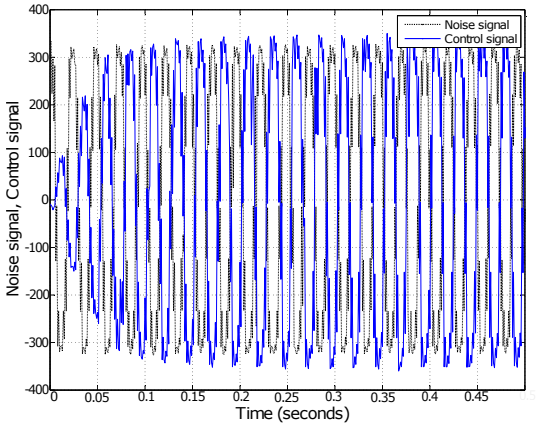

(a) Control signal for $\mu = \mu_a$

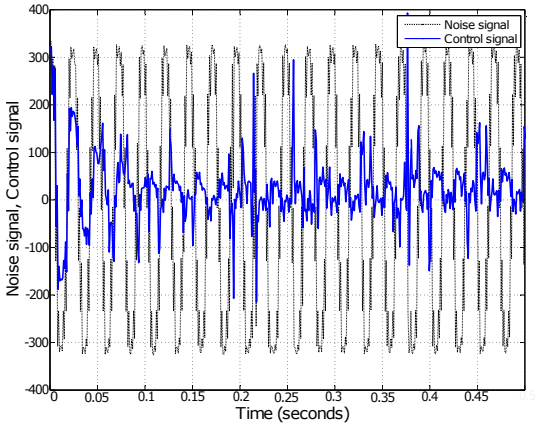

(b) Residual Error for $\mu = \mu_a$

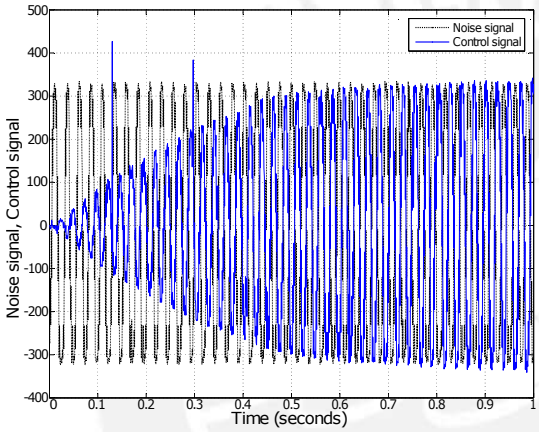

(c) Control signal for $\mu = \mu_b$

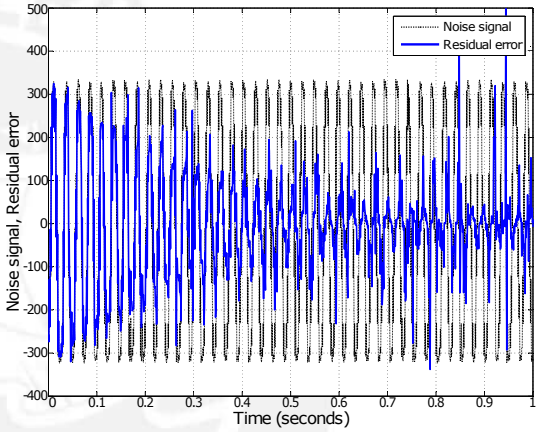

(d) Residual Error for $\mu = \mu_b$

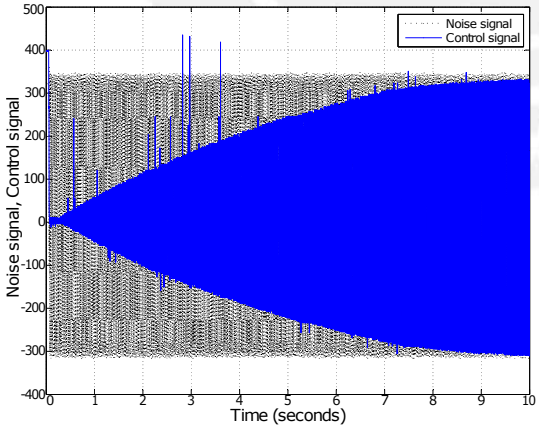

(e) Control signal for $\mu = \mu_c$

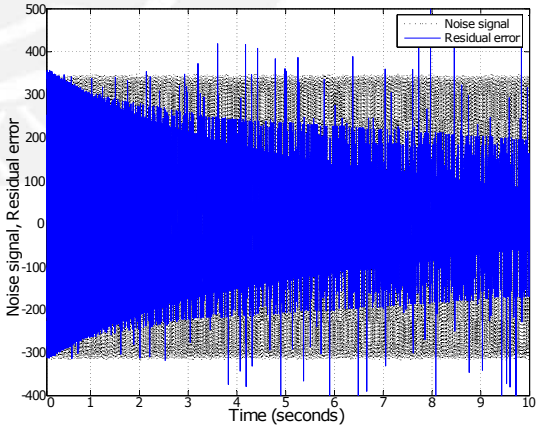

(f) Residual Error for $\mu = \mu_c$

Figure 4.11: Results for additional values of μ

Conclusions

1. The present research has optimized a Delayed FxLMS algorithm for a prototype of ANC system, through the calculus of the optimal step-size.
2. Approximation developed by Widrow *et al* in **??** for a Single Frequency ANC system, which is a non-linear system, in a transfer function shows a considerable accuracy in order to analyse system response.
3. Single Frequency ANC system can be considered the most simple ANC system because require the lowest order filter (second order) in order to be controlled.
4. The main elements which can improve the performance of the Single Frequency FxLMS algorithm, according the transfer function of Widrow *et al*, are the step-size μ and differences between the secondary path effect and its estimation.
5. The present work has obtained the operation interval of the step-size μ for a Single Frequency ANC system considering the stability conditions of the approximate system. Additionally, it has been achieved the response variation according to the μ displacement in the mentioned interval.

Recommendations

1. In this work, the experiment test have been developed in the ARDUINO UNO device, which IC ATmega48A presents 10-bits Analog to Digital Converter (ADC) resolution and low ADC speed. Despite of that this research pretends to minimize computational costs, it is recommendable to use a little more complex device in order to obtain better results.

Bibliography

[AAK07] Muhammad Tahir Akhtar, Masahide Abe, and Masayuki Kawamata. On active noise control systems with online acoustic feedback path modeling. *Audio, Speech, and Language Processing, IEEE Transactions on*, 15(2):593–600, 2007.

[BH09] David A Bies and Colin H Hansen. *Engineering noise control: theory and practice*. CRC press, 2009.

[BM12] Leo L Beranek and Tim Mellow. *Acoustics: sound fields and transducers*. Academic Press, 2012.

[CC15] Jesús Alan Calderón Chavarri. Analysis and implementation of active noise control strategies using piezo and eap actuators. 2015.

[Egg13] Jos J Eggermont. *Noise and the brain: experience dependent developmental and adult plasticity*. Academic Press, 2013.

[Fuc13] Helmut V Fuchs. *Applied Acoustics: Concepts, Absorbers, and Silencers for Acoustical Comfort and Noise Control: Alternative Solutions-Innovative Tools-Practical Examples*. Springer Science & Business Media, 2013.

[GRMP13] Fernando Gonzalez, Roberto Rossi, German R Molina, and Gustavo Parlanti. Fxlms and mfxlms stability constrains when used in active noise control. *IEEE Latin America Transactions*, 11(1):213–217, 2013.

[Han02] Colin N Hansen. *Understanding active noise cancellation*. CRC Press, 2002.

[HSQ+12] Colin Hansen, Scott Snyder, Xiaojun Qiu, Laura Brooks, and Danielle Moreau. *Active control of noise and vibration*. CRC Press, 2012.

[KBM13] Branko Kovacevic, Zoran Banjac, and Milan Milosavljevic. *Adaptive Digital Filters*. Springer Publishing Company, Incorporated, 2013.

[KGK12] Yoshinobu Kajikawa, Woon-Seng Gan, and Sen M Kuo. Recent advances on active noise control: open issues and innovative applications. *APSIPA Transactions on Signal and Information Processing*, 1:e3, 2012.

[KKG10] Sen M Kuo, Kevin Kuo, and Woon Seng Gan. Active noise control: open problems and challenges. In *Green Circuits and Systems (ICGCS), 2010 International Conference on*, pages 164–169. IEEE, 2010.

[KM99] Sen M Kuo and Dennis R Morgan. Active noise control: a tutorial review. *Proceedings of the IEEE*, 87(6):943–973, 1999.

[Mös09] Michael Möser. *Engineering acoustics: an introduction to noise control*. Springer Science & Business Media, 2009.

[Pir15] Luigi Piroddi. Active noise control: Course notes. Diparimento di Electtronica e Informazione. Politecnico di Milano, 2015.

[Sia12] Daniela Siano. *Noise Control, Reduction and Cancellation Solutions in Engineering*. Intech, 2012.

[Sny12] Scott D Snyder. *Active noise control primer*. Springer Science & Business Media, 2012.

[WGM+75] Bernard Widrow, John R Glover, John M McCool, John Kaunitz, Charles S Williams, Robert H Hearn, James R Zeidler, JR Eugene Dong, and Robert C Goodlin. Adaptive noise cancelling: Principles and applications. *Proceedings of the IEEE*, 63(12):1692–1716, 1975.

[ZJ89] Eldon Ziegler Jr. Selective active cancellation system for repetitive phenomena, October 31 1989. US Patent 4,878,188.